frontiers in Physics

REVIEW
published: 21 April 2015
doi: 10.3389/fphy.2015.00026

Imaging spin dynamics on the nanoscale using X-Ray microscopy

Hermann Stoll[1], Matthias Noske[1], Markus Weigand[1], Kornel Richter[2], Benjamin Krüger[2], Robert M. Reeve[2], Max Hänze[3], Christian F. Adolff[3], Falk-Ulrich Stein[3], Guido Meier[3,4,5], Mathias Kläui[2] and Gisela Schütz[1]*

[1] Moderne Magnetische Systeme, Max-Planck-Institut für Intelligente Systeme, Stuttgart, Germany, [2] Institut für Physik, Johannes Gutenberg-Universität Mainz, Mainz, Germany, [3] Institut für Nanostruktur- und Festkörperphysik, Universität Hamburg, Hamburg, Germany, [4] The Hamburg Centre for Ultrafast Imaging, Universität Hamburg, Hamburg, Germany, [5] Max-Planck-Institut für Struktur und Dynamik der Materie, Hamburg, Germany

The dynamics of emergent magnetic quasiparticles, such as vortices, domain walls and bubbles are studied by scanning transmission X-ray microscopy (STXM), combining magnetic (XMCD) contrast with about 25 nm lateral resolution as well as 70 ps time resolution. Essential progress in the understanding of magnetic vortex dynamics is achieved by vortex core reversal observed by sub-GHz excitation of the vortex gyromode, either by ac magnetic fields or spin transfer torque. The basic switching scheme for this vortex core reversal is the generation of a vortex-antivortex pair. Much faster vortex core reversal is obtained by exciting azimuthal spin wave modes with (multi-GHz) rotating magnetic fields or orthogonal monopolar field pulses in the x and y direction, down to 45 ps in duration. In that way unidirectional vortex core reversal to the vortex core "down" or "up" state only can be achieved with switching times well below 100 ps. Coupled modes of interacting vortices mimic crystal properties. The individual vortex oscillators determine the properties of the ensemble, where the gyrotropic mode represents the fundamental excitation. By self-organized state formation we investigate distinct vortex core polarization configurations and understand these eigenmodes in an extended Thiele model. Analogies with photonic crystals are drawn. Oersted fields and spin-polarized currents are used to excite the dynamics of domain walls and magnetic bubble skyrmions. From the measured phase and amplitude of the displacement of domain walls we deduce the size of the non-adiabatic spin-transfer torque. For sensing applications, the displacement of domain walls is studied and a direct correlation between domain wall velocity and spin structure is found. Finally the synchronous displacement of multiple domain walls using perpendicular field pulses is demonstrated as a possible paradigm shift for magnetic memory and logic applications.

Keywords: spin waves, domain walls, vortex dynamics, nano wires, X-ray microscopy, vortex core reversal, coupled modes, spin-transfer-torque

OPEN ACCESS

Edited by:
Hendrik Ohldag, SLAC National Accelerator Laboratory, USA

Reviewed by:
Jeffrey McCord, Kiel University, Germany
Peter Varga, Vienna University of Technology, Austria

****Correspondence:***
Hermann Stoll, Moderne Magnetische Systeme, Max-Planck-Institut für Intelligente Systeme, Heisenbergstr. 3, 70569 Stuttgart, Germany
stoll@is.mpg.de

Specialty section:
This article was submitted to Condensed Matter Physics, a section of the journal Frontiers in Physics

Received: *15 January 2015*
Paper pending published: *09 February 2015*
Accepted: *30 March 2015*
Published: *21 April 2015*

Citation:
Stoll H, Noske M, Weigand M, Richter K, Krüger B, Reeve RM, Hänze M, Adolff CF, Stein F-U, Meier G, Kläui M and Schütz G (2015) Imaging spin dynamics on the nanoscale using X-Ray microscopy. Front. Phys. 3:26. doi: 10.3389/fphy.2015.00026

1. Introduction

Recently the physics of surfaces, interfaces and nanostructures has become one of the major areas of research, due to the trend in science and technology toward miniaturization of physical systems into the nanoscale. From the scientific viewpoint, such systems pose a whole new set of problems, both

theoretical and experimental. Fundamentally, novel properties emerge in magnetic elements as the lateral structure dimensions become comparable to or smaller than certain characteristic length scales, such as spin diffusion length, carrier mean free path, magnetic exchange length, domain wall width, etc. The effects of the governing energy terms determine the interplay between the relevant physical length scales and the sizes of the structured materials. When the geometry changes from the bulk to the nanoscale, the magnetic properties of ferromagnetic elements start to be governed by the element geometry and not only by the intrinsic materials properties. Such behavior and in particular the magnetization configurations and reversal in small magnetic elements have been reviewed in detail for instance in Hubert and Schäfer[1] Kläui and Vaz[2]. Such a strong dependence on the geometry allows one then to tailor the magnetization configuration and spin switching by appropriately engineering the geometry. The magnetization configuration that constitutes the lowest energy state in a small magnetic structure can for instance be set to a multidomain state with vortices or domain walls, since the dipolar interaction (stray field) leads to the magnetization being parallel to the element edges, which then results in a very reproducible and controllable spatially inhomogeneous magnetization distribution (domain configuration). To study such geometrically confined magnetization configurations, direct imaging is the method of choice, as it allows one to deduce the spatially resolved spin structure with high resolution. Furthermore, the geometrical confinement and the resulting topology of the spin structures leads to intricate dynamics and to study this, dynamic imaging methods are needed. X-ray based microscopy provides the right tools, as X-rays can be produced in short bunches providing time resolution and the short wavelength combined with the dichroism magnetic contrast mechanism provides the necessary spatial resolution for high resolution dynamic magnetic imaging [3–6]. Here we focus on selected experiments performed primarily by our groups describing the dynamics of some of the basic magnetic spin structures present in soft magnetic materials patterned onto the nanoscale: first the magnetic vortex and arrays of vortices, then domain walls, which are compound quasiparticles that can include vortices and other spin structures and finally bubble skyrmions that comprise two domains delinated by a domain wall.

2. Dynamics of Magnetic Vortices

2.1. Sub-100 ps Vortex Core Reversal

The magnetic vortex state is well known as the simplest, nontrivial ground state configuration in geometrically confined micron and sub-micron sized ferromagnetic discs or platelets [1, 8–10] and therefore an interesting subject for the study of micromagnetism. It consists of an in-plane curling magnetization, with two possible circulations[1], $c = +1$ and $c = -1$, which in the center, in order to avoid a singularity, turns out-of-plane and forms the vortex core. The vortex core has a radius of about 10–20 nm and plays a key role in the magnetization dynamics of vortex structures [11–15]. As the out-of-plane magnetization of the vortex core polarization p can point in two directions, either "up" or "down" ($p = +1$ or -1), it could be regarded as memory element. The high stability of the vortex structure and its very low stray fields would offer distinct advantages for applications requiring high density integration. Switching of the vortex core can be achieved, for instance, by applying a magnetic field perpendicular to the sample plane. However, field strengths of about 0.5 T are reported to be necessary to crush the vortex core in this way and to rebuild it in the opposite direction [16, 17]. Such high fields are intricate to realize on the small length scales necessary in practical devices for data storage. The discovery of low-field vortex core reversal by excitation of the (sub-GHz) vortex gyromode [7] triggered a new chapter in magnetic vortex dynamics. It could be demonstrated experimentally, by time-resolved X-ray microscopy as sketched in **Figure 1**, that the vortex core can be reversed with bursts of an alternating linear magnetic field with an amplitude as low as 1.5 mT (which has to be compared with the 0.5 T mentioned above). Based on micromagnetic simulations it was suggested that this switching scheme is mediated by the creation and annihilation of vortex-antivortex (VA) pairs [7]. Later the first step of this mechanism was proved experimentally [18]. This VA mediated switching scheme for low-field vortex core reversal is now generally accepted in the community [19–23]. The VA mechanism for easy vortex core reversals seems to be universal and independent of the type of excitation as the excitation can be performed not only by magnetic ac field bursts, but also by magnetic mono-pulses [24] or spin-transfer torque (STT) [25, 26]. So far experiments have been performed with linear field pulses or bursts which toggle the vortex core from "up" to "down" and vice versa. For data storage application an unequivocal switching direction would be highly desirable. This could be achieved by an excitation with micron sized circular rotating fields [27, 28]. In-plane rotating magnetic fields were produced by cross-shaped striplines below the samples. Clockwise (CW) or counter-clockwise (CCW) senses of rotation can be generated by ac currents in the horizontal and vertical direction with the same frequency but a $+90$ or -90 phase difference respectively. The vortex core movement could only be excited with the correct sense of rotation (CW or CCW) of the external rotating field depending on the vortex core polarization [27, 28]. When the amplitude of the rotating field was increased above a distinct threshold the gyrotropic vortex motion stopped, indicating that the vortex core polarization has been switched. For re-switching an external field with the opposite sense of rotation had to be applied. All these results are consistent with micromagnetic simulations showing that an unequivocal and unidirectional switching of the vortex core polarization can be achieved by circular field excitation. Magnetic anti-vortices also could be switched unidirectionally with rotating spin currents [29] or magnetic fields [30].

Surprisingly, significant differences have been found in the ac field amplitudes needed for switching the vortex polarization from "up" to "down" and from "down" to "up" [27]. Such differences were never observed so far in micro-magnetic simulations of "perfect" samples. It could be shown that the surface roughness

[1]In some previous papers the sense of rotation of the in-plane magnetization "c" is denoted as "chirality," an expression which should be better assigned to the "real" handedness, the product "cp."

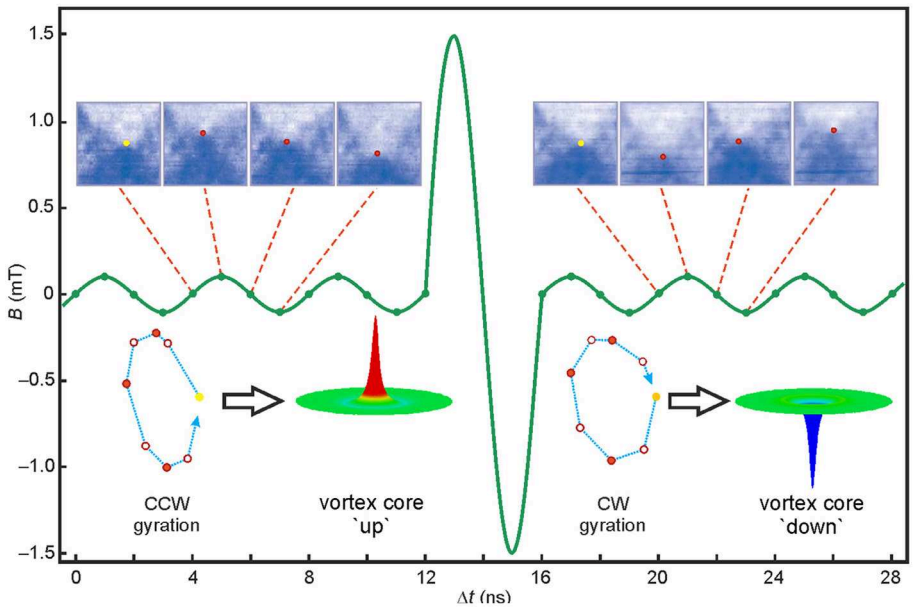

FIGURE 1 | Switching or the vortex core by excitation of the vortex gyromode at 250 MHz with a single period burst at an amplitude of 1.5 mT [7]. Permalloy sample: 1.5 μm in diameter, 50 nm thick. Before and after the switching the vortex polarization p was probed by imaging the sense of rotation of the vortex gyration by time-resolved X-ray microscopy (CCW for vortex core "up," CW for vortex core "down").

of real samples is responsible for this symmetry breaking [18]. In addition, it should be noted, that not only the vortex polarization "p" but also the circulation "c" can be switched dynamically [31].

So far the vortex core was reversed by excitation of the sub-GHz vortex gyromode of the vortex structure. At much higher (multi-GHz) frequencies, vortex structures possess azimuthal spin wave eigenmodes arising from the magneto-static interaction. They are characterized by a radial mode number n and an azimuthal mode number m. The interaction between the spin modes ($n > 0$, $|m| = 1$) and the gyrotropic mode leads to a frequency splitting Δf of modes with opposite rotation senses as illustrated in **Figure 2**. By exciting the vortex structure with bursts of GHz rotating magnetic fields the vortex core polarization could be reversed. Such measurements have been performed at the scanning transmission X-ray microscope (STXM) at BESSY II, Berlin [3, 4]. **Figure 3** (upper part) shows experimentally observed vortex core switching from the initial state "up" to "down" as a function of excitation frequency and amplitude as well as the sense of rotation of the external field. Distinct regions are observed in a Permalloy disc, 1.6 μm in diameter, 50 nm thick, showing minima in the switching amplitude for both CW excitation (blue color) and for CCW excitation (red color). These regions can be assigned to distinct spin wave modes as sketched in the middle part of **Figure 3**. The lower part of **Figure 3** shows the results of our micromagnetic simulations [3, 4] which are in good agreement with the experimental results. Toggling of the vortex core from "down" back to "up" at the same frequency can be achieved only if the sense of rotation of the external rotation field is reversed. This allows unidirectional switching at GHz frequencies similar to that demonstrated for the sub-GHz gyrotropic mode before, but much faster. It was also found that the vortex displacement caused by spin wave excitation is an order of magnitude smaller compared to what is needed to switch the core by the (sub-GHz) gyration mode [3, 4]. This reduces the time of the system needed to relax back into its ground configuration after a switching event occurred.

In Reference [3] 24 periods of GHz excitation have been applied. By using a shorter excitation, only one period of a rotating GHz magnetic field, the vortex core could be switched in about 200 ps in Permalloy samples with a diameter of 1.6 μm, 50 nm thick, even if the excitation time itself is shorter [32]. It was found that the switching time is limited by the time needed for the transport of the homogeneously distributed excitation energy to the center of the sample [33].

Noske et al. [34] have demonstrated how to speed up spin wave mediated unidirectional vortex core reversal to below 100 ps. In order to overcome the 200 ps limitation [32, 33] smaller samples have been used, i.e., Permalloy disks with a diameter of 500 nm and a thickness of 50 nm, excited with an orthogonal sequence of monopolar pulses in the x and y direction. The experimental pulse length T varied from 45 ps to 90 ps (FWHM) and the delay between the two pulses was tuned to 1/2 T as sketched in the upper part of **Figure 4**. For a counter clockwise (CCW) sense of rotation (**Figures 4A,B**), where the pulse B_x in the x-direction starts before the pulse B_y in the y-direction, it was found that the switching threshold for an initial vortex core "down" is nearly twice as high as for an initial vortex core "up." This asymmetry in the switching threshold (**Figure 4**) is nearly independent of the pulse length and proves the undirectionality of the process for field strengths of about 15–30 mT. In **Figures 4C,D** the

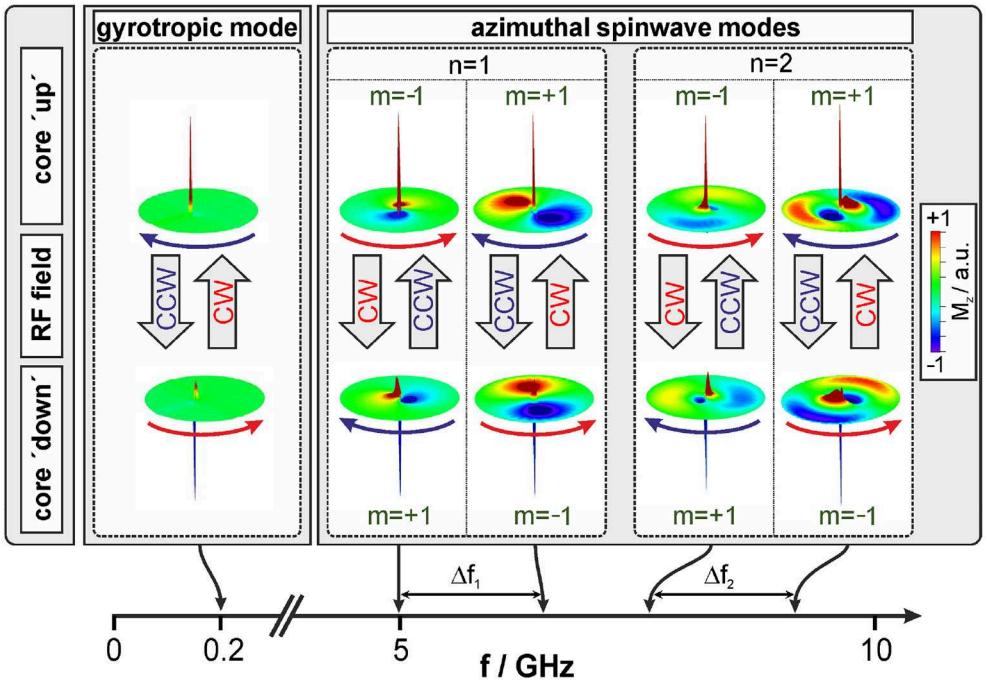

FIGURE 2 | Unidirectional vortex core reversal by excitation of the (sub-GHz) gyromode or (multi-GHz) azimuthal spin waves with external rotating magnetic fields [3]. Using 24 periods for excitation [3] switching only occurs if the frequency and the senses of rotation are the same for the specific mode and the external field.

timing of the pulse sequence is inverted so that B_y starts before B_x which leads to a clockwise (CW) excitation. Due to symmetry reasons, a vortex core "up" ("down") excited with a CW sequence is expected to have the same switching behavior as a vortex core "down" ("up") excited by a CCW sequence. This is confirmed in the experiment (C,D) proving that the pulse sequence (CW or CCW) dependent switching behavior is not just a result of, e.g., sample imperfections.

Our experimental results (**Figures 4A–D**) demonstrate that highly reliable unidirectional switching is possible experimentally with pulse lengths of only 45 ps and total excitation times as short as 70 ps which is the fastest value shown for unidirectional vortex core reversal so far. Three-dimensional micromagnetic simulations have been performed [34] with the OOMMF code [35]. The results are shown in **Figures 4E,F** and demonstrate a good qualitative agreement with the experimentally observed asymmetry in switching thresholds. For high pulse amplitudes a region (shaded area) exists in the phase diagram where the vortex core polarization after excitation is the same as before. Analyzing the corresponding simulations of **Figure 4E**, this can be attributed to double switching events. For further increased amplitudes even triple switching is observed.

The switching time could be derived from micromagentic simulations [34], not only for samples with a diameter of 500 nm (as used for the measurements) but also for smaller samples, 250 nm and 125 nm in diameter. For all these three diameters unidirectional switching could be achieved within a minimum switching time of 70–75 ps, defined from the start of the excitation (50% of the full amplitude) until the vortex core is completely reversed. However, for smaller samples higher excitation amplitudes are needed [34]. In order to get more insight into the dynamics of the reversal process the out-of-plane component of the magnetization during the switching process has been imaged experimentally by time-resolved scanning transmission X-ray microscopy and these results have been compared with those of corresponding micromagnetic simulations [34]. Measurements and simulations show excellent agreement (**Figure 5**). The vortex core is initially pointing up (red dot). In the following $t = 0$ ps corresponds to the point in time when the first pulse B_x reaches fifty percent of its maximum amplitude (see **Figure 5**, lower part). A pulse length T of 60 ps and a total excitation length of 90 ps was applied. During the rising edge of the first pulse, a bipolar structure forms similar to an $n = 1$, $m = +1$ spinwave. The counter clockwise rotation of this structure follows the rotational sense of the exciting magnetic field. The region where the magnetization points down (the "dip") gets localized at the core region until the vortex core is reversed at $t = 98$ ps (dashed box).

In conclusion, unidirectional vortex core reversal can be achieved by highly non-resonant pulsed excitation with pulse lengths T between 90 and 45 ps [34]. From micromagnetic simulations a field-strength dependent switching time has been deduced well below 100 ps [34]. The time development of the out-of-plane magnetization was imaged by time-resolved X-ray microscopy which agrees excellently with the results from a corresponding micromagnetic simulation. A comparison of the magnetization profiles for CCW and CW excitation and the

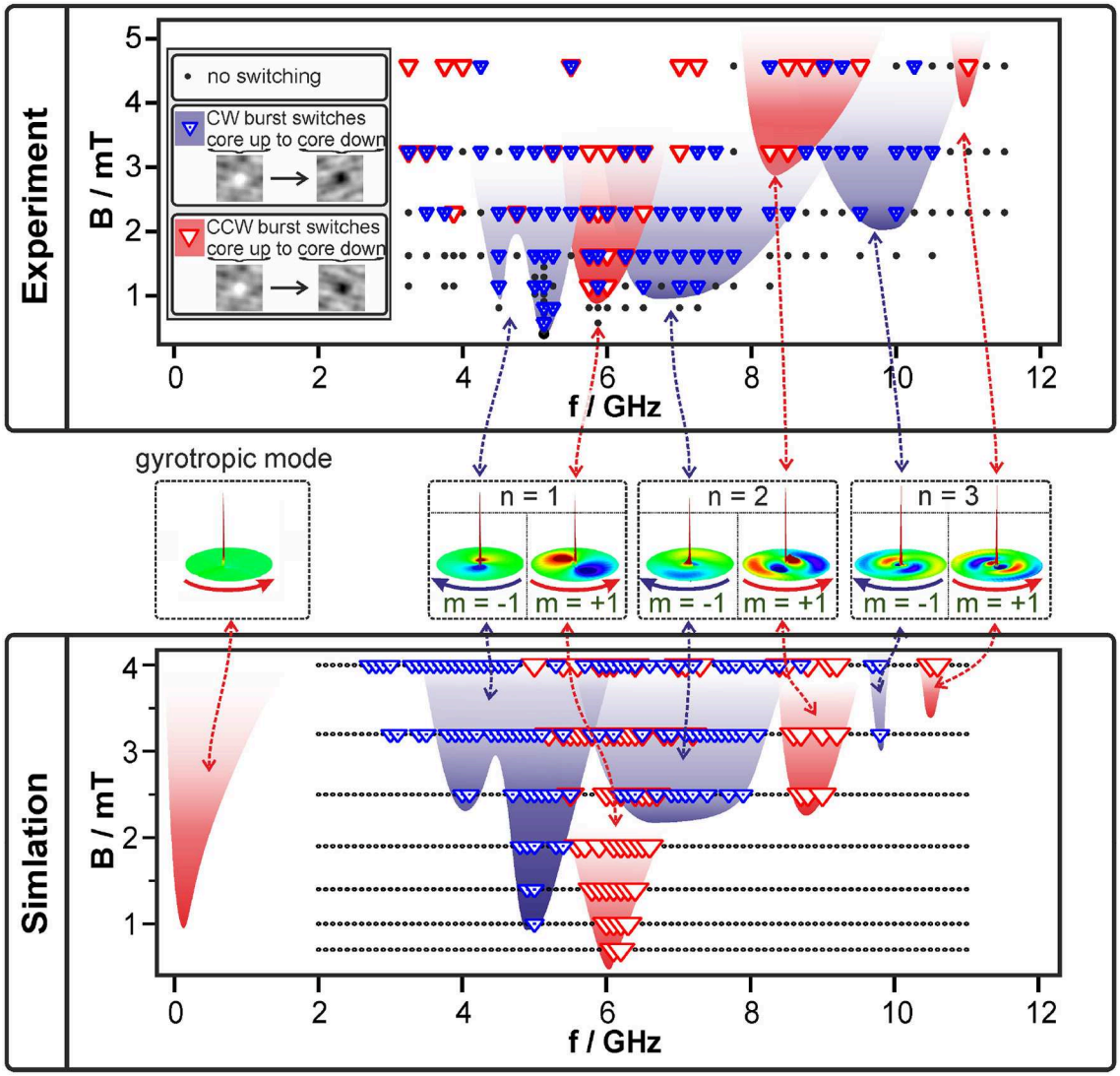

FIGURE 3 | Phase diagram of spin wave mediated vortex core reversal: switching amplitude versus excitation frequency for excitation with rotating external magnetic fields with a duration of 24 periods [3, 4]. A CW (marked blue) or a CCW (marked red) sense of rotation has to be applied for low-field switching in accordance with the sense of rotation of the spin wave modes to be excited.

corresponding vortex core trajectories show a clear asymmetry [34]. Here, in contrast to resonant energy coupling into one single CW or CCW rotating spin wave mode [3], the unidirectional switching is based on different core trajectories leading to different "dip" formations for CW and CCW excitation and resulting in core reversal at low fields for one core polarization only [34]. This unidirectionality and the high speed of the process might open up new possibilities for spintronics applications.

2.2. Magnonic Vortex Crystals

Coupled modes play a fundamental role in solid state physics. For example the propagation of sound waves in crystals can be described by coupled harmonic oscillators. Although the interactions, in such models, may be limited to the next neighbors of a lattice site, the vast number and the order of all participating oscillators determines the actual behavior [36, 37]. Recently, it has been demonstrated that the concept of coupled harmonic oscillators is applicable to a system of coupled magnetic vortex oscillators [38–40]. The gyrotropic mode representing the fundamental excitation of the vortex ground state corresponds to a gyration of the vortex core around the center region of the disk and can be compared to the oscillation of a harmonic oscillator [7]. Coupling occurs when the center-to-center distance of a pair of vortices is less than about twice the diameter of the disks [41, 42]. Vortex oscillations have been studied in pair-coupled vortices [43–45], in one-dimensional vortex chains [46] and larger two dimensional vortex arrays [47, 48]. In contrast to systems of coupled harmonic oscillators the interaction strength can be tuned dynamically in dependence on the

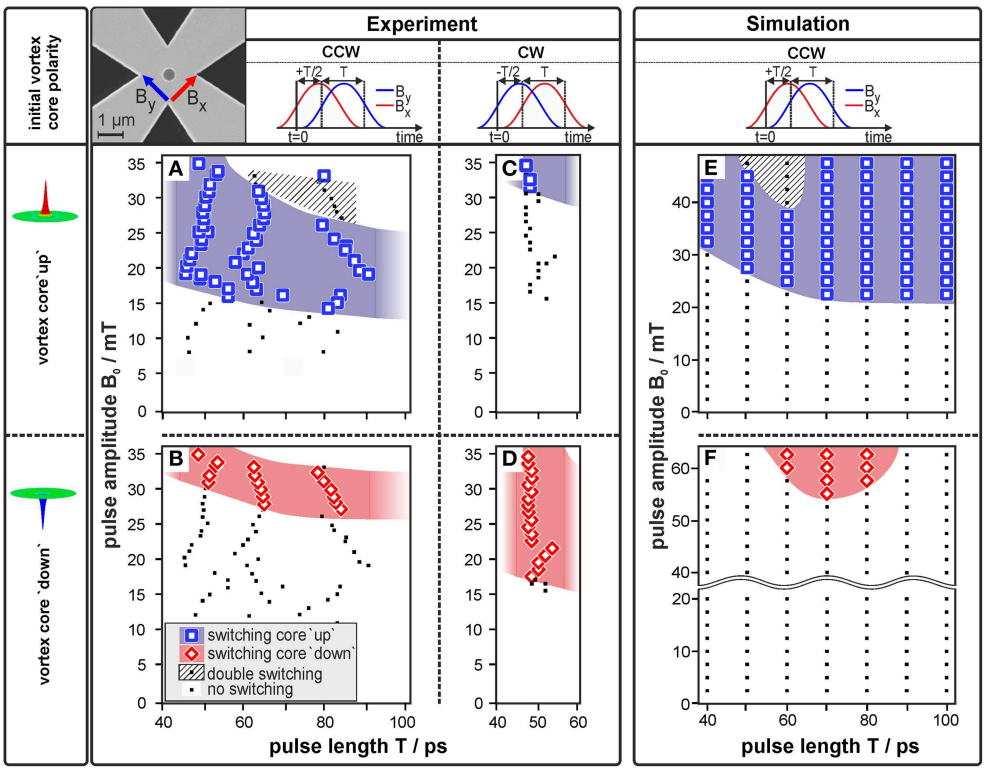

FIGURE 4 | Phase diagrams for vortex core reversal by pulsed excitation: experiments (A–D) and micromagnetic simulations (E,F) [34]. Unidirectional reversal is found in a broad region, where CCW excitation switches the vortex core if the initial core is "up" **(A,E)** but no switching occurs if the vortex core is "down" **(B,F)**. For CW excitation, this behavior is inverted **(C,D)** as expected for symmetry reasons. A scanning electron microscope image of the crossed striplines with the Permalloy disk is shown in the upper left corner. The arrows indicate the directions of the magnetic field pulses as sketched in the upper row.

polarizations [49, 50]. Distinct polarization configurations can be tuned using a mechanism called self-organized state formation [51]. This allows for the manipulation of the properties of a magnonic vortex crystal by a temporary application of magnetic fields. Such tunable vortex crystals are suitable for potential applications like wave transmission media or magnetic storage devices.

The motions of vortex crystals are theoretically accessible by the Thiele approach. The Thiele equation describes the motion of a magnetic vortex in a particle model [52, 53],

$$(G_0^2 + \alpha^2 D_0^2)\dot{\vec{x}} = \vec{G} \times \vec{F} - \alpha D_0 \vec{F}, \qquad (1)$$

where $\vec{x} \in \{\vec{x}_1, ..., \vec{x}_N\}$ is the displacement of a vortex core, G_0 is the absolute value of the gyrovector $\vec{G}$ [52], $\vec{F}$ is the force pointing perpendicular to the direction of motion and N is the number of vortices in the system. In the absence of external fields the vortex cores oscillate with their eigenmodes. In this undriven case the Thiele equation can be transformed into a system of first order linear differential equations with solutions of the form $\vec{u} = \vec{v}e^{\lambda t}$ [38],

$$\dot{\vec{u}} = -\frac{\tilde{p}}{G_0}\tilde{R}_{90}(\kappa \mathbb{1} + \tilde{Z})\vec{u} =: \tilde{M}\vec{u}. \qquad (2)$$

Here, the system of Thiele equations has been reduced to an eigenvalue problem $\tilde{M}\vec{v} = \lambda\vec{v}$, where λ are eigenvalues and $\vec{v}$ are eigenvectors of the system. The vortex motions $\vec{u} = (\vec{x}_1, \vec{x}_2, ..., \vec{x}_N)$ depend on the polarizations of the vortices $\tilde{p}$, the stiffness coefficient of the harmonic potential κ and the interaction matrix $\tilde{Z}$ as described in Hänze [38]. For this system, eigenvalues represent the frequencies and eigenvectors the motions for any alignment of vortices. In the case of a 3 x 3 vortex crystal nine coupled vortex oscillators result in nine independent eigenmodes. The polarization of every single vortex influences the eigenfrequencies of the crystal. Nine coupled vortices lead to a number of $2^9 = 512$ possible polarization patterns. The eigenmodes of each pattern differ from one another. For this reason we focus on one polarization pattern to illustrate the possible eigenmodes and frequencies. This pattern has columns of alternating polarizations and will be addressed as stripe pattern. We obtain nine eigenmodes that are depicted in **Figure 6** with its frequencies and motions. The motions are characterized by the relative phases and the relative amplitudes between the vortices during one oscillation period. The phases indicate the positions of the vortices for a snapshot in time. Eigenfrequencies are scattered around the resonance frequency of 238 MHz for an isolated vortex (see **Figure 6B**). For some eigenmotions the amplitude of a vortex is completely suppressed, for example for the

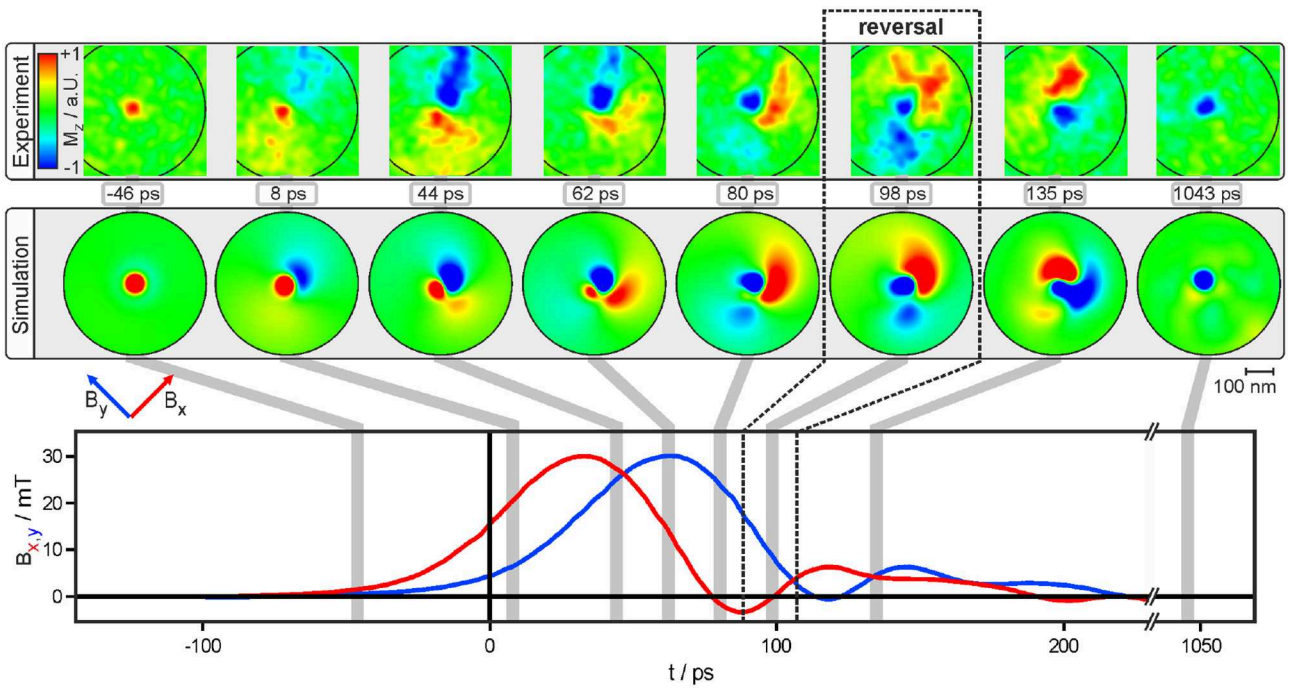

FIGURE 5 | Imaging of the vortex core reversal process by the excitation with orthogonal magnetic field pulses, experiment and micromagnetic simulation [34]. Pulse amplitude: 30 mT, pulse width 60 ps, total duration of the excitation: 90 ps (see lower row). The upper row shows the dynamic response of the out-of-plane magnetization measured with time-resolved scanning transmission X-ray microscopy. The middle row shows results from the corresponding micromagnetic simulation (folded with the experimental temporal and lateral resolution) which is in good agreement with the experimental data.

central vortex of mode 2 (see **Figure 6C**). Other modes have comparable amplitudes but different phase relations. We have to keep in mind, that the sense of rotation depends on the polarization. Consequently the phase relations between vortices with negative and positive polarization change along a period of rotation. Although the circulations do not alter the eigenfrequencies they result in a phase shift of 180°. Accordingly **Figure 6C** shows snapshots of the phase relations of an array with equal circulations.

There are nine eigenmotions and eigenfrequencies for the polarization pattern described in **Figure 6**. But not all of the modes can efficiently be excited when an alternating field is applied to all disks in the crystal equally (see **Figure 6A**). A single vortex that is excited by a unidirectional alternating field in y-direction $\vec{H} = (0, \sin(\omega t))$ gyrates according to $\vec{x} \propto (c\cos(\omega t), cp\sin(\omega t))$. Since the vortex crystal is a weakly coupled system, the exciting field allows only small deviation from this enforced phase relation. Thus, eigenmodes that resemble the enforced relative phases are excited more efficiently. Those modes are excited at the corresponding eigenfrequency. Since the eigenmodes depend on the polarization pattern, different patterns vary in their frequency of most efficient excitation. E.g., for the stripe pattern depicted in **Figure 6C** mode 1 resembles almost perfectly the enforced phase relation so that the frequency of most efficient excitation will be around the corresponding eigenfrequency of 228 MHz. When the pattern is rotated by 90°, mode 7 resembles the enforced phase relation, and the pattern will efficiently be excited at 242 MHz. **Figure 7A** shows calculated absorption profiles for all 512 possible polarization patterns, when the damping of the system is considered reasonably [51]. The absorption is proportional to the mean squared velocity of all vortices, when an alternating magnetic field in the y-direction is applied to the whole crystal. The two orientations of the pattern with lines of constant polarization are highlighted in red and blue. One can see that they indeed differ in their frequency of most efficient excitation. Horizontal lines of constant polarization can be excited efficiently around 228 MHz and vertical lines at about 242 MHz. When a pattern is excited efficiently, the vortices in the crystal reach high velocities. At a critical velocity of about 250 ms^{-1} [54] the vortices switch their polarizations and thereby lead to another polarization pattern in the crystal. The critical velocities can be reached when the amplitude of the exciting field is increased. At a critical field amplitude, only the least efficiently excitable polarization pattern will not switch. Starting from a random pattern, this least efficiently excitable pattern will be tuned after several switching processes. In the experiments we use an adiabatic reduction of the field amplitude in order to tune a polarization state in the crystal. The vortices switch rather randomly at high amplitudes of the harmonic field that is applied to all magnetic vortices in the crystal via an alternating current that is sent through a stripline above the crystal. At intermediate field amplitudes the switching stops when certain stable polarization

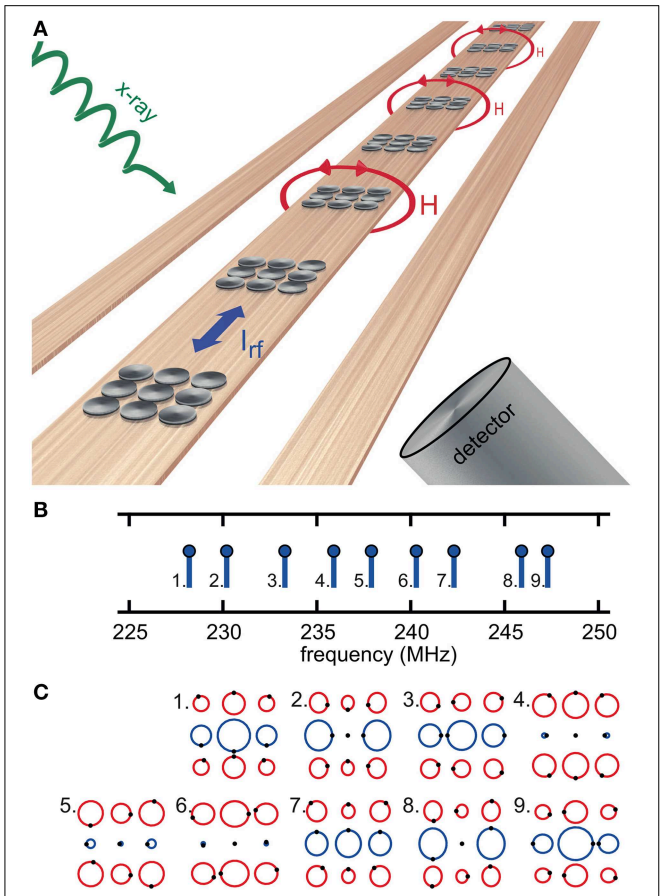

FIGURE 6 | (A) Vortex arrays investigated with transmission soft X-ray microscopy. The magnetic field *H* is applied via an alternating current send through a coplanar waveguide. The disks have a diameter of 2 μm and a center-to-center distance of 3 μm. The thickness of the disks is 60 nm. **(B)** Calculated eigenfrequencies of the polarization pattern with columns of alternating polarization. **(C)** Trajectories of the eigenmodes. Phase relations of the depicted snapshot are indicated by black dots. The polarization is color-coded (red and blue for up and down) to indicate the sense of rotation.

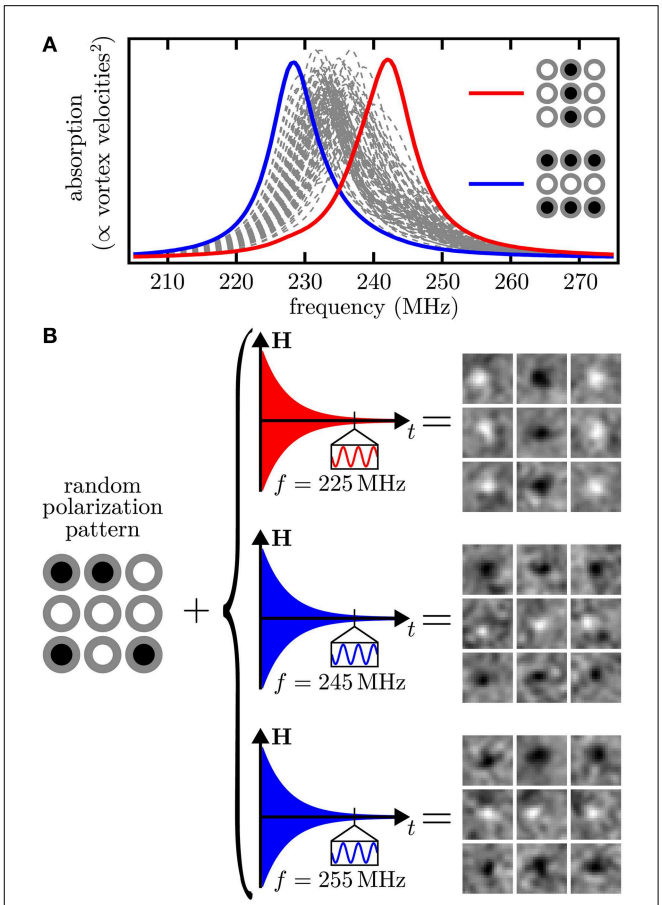

FIGURE 7 | (A) Calculated absorption profiles of the magnonic vortex crystal for all possible polarization patterns. The patterns with lines of constant polarizations are highlighted in red and blue. **(B)** Experimental results for the self-organized state formation. Starting from a random configuration, ordered polarization patterns are tuned by an adiabatic reduction of a high-frequency magnetic field. The obtained patterns depend on the frequency of excitation.

configurations are reached eventually [51]. The resulting state of this self-organized state formation depends on the frequency of excitation. As can be seen in **Figure 7A** the least efficiently excitable state is the vertical line pattern for frequencies below 235 MHz and the horizontal line pattern for higher frequencies. Thus, the vertical line pattern is tuned at low frequencies and the horizontal line pattern at high frequencies. The experimental results presented in **Figure 7B** correspond to the predicted states. The vertical line pattern is tuned at low frequency of 225 MHz and the horizontal line pattern is tuned for two higher frequencies of 245 MHz and 255 MHz. For the presented system only two polarization states can be tuned. The states that are accessible via self-organized state formation depend on the coupling strength between the vortices. Thus, when the disk interspace is reduced, additional patterns can be tuned [51].

The concept of eigenmodes in magnonic vortex crystals can be used to understand the excitability of magnonic vortex crystals with alternating unidirectional magnetic fields. Such an external magnetic field mainly excites eigenmodes that resemble a specific phase relation between the vortices and the exciting field. The vortices are excited efficiently, when the frequency of excitation is close to the eigenfrequencies of those eigenmodes. An adiabatic reduction of a high-frequency magnetic field excitation leads to self-organized relaxation of the system into well-ordered states. The emerging states are the least efficiently excitable states at the corresponding frequency.

3. Magnetic Domain Wall Dynamics

Next we go from the simple vortex, which constitutes the lowest energy state for many disc geometries to spin structures in elongated elements. In long magnetic wires (we consider here soft magnetic flat strips where the length >> width >> thickness) the lowest energy state is the single domain state with the magnetization pointing uniformly along the wire axis. The simplest non-trivial (inhomogeneous) magnetization configuration is a state with magnetic domains and domain walls (DWs).

Domain walls, which constitute the boundary between domains, have been intensively researched in the past, though with a focus on the domain wall types that occur in the bulk or in continuous films. The most prominent examples are the Bloch and the Néel wall types, which occur in continuous thin films [1, 55]. In soft magnetic materials wires and related geometries, such as rings, two types of domain walls occur: transverse and vortex walls [55–57]. These DWs can be considered as confined spin structures with quasiparticle properties that exhibit complex dynamics when excited. Whilst electrical measurements based on e.g., anisotropic magnetoresistance or the extraordinary Hall effect provide an easy and fast way to probe the presence of DWs in a structure, magnetic imaging is vital to provide an in-depth understanding of the systems. In particular, since the dynamic behavior of these objects is intricately linked to the internal spin-structure, the high resolution imaging of the spin state is of paramount importance. As the first step, the static domain wall spin structures have been imaged. For soft magnetic Permalloy and polycrystalline Co X-ray magnetic circular dichroism photoemission electron microscopy [XMCD-PEEM [5, 6]] has been employed in order to extract the phase-diagram which describes the relation between the geometry of the wire and the DW type [56, 58, 59]. In general the transverse wall is stable for narrower and thinner wires, whereas the vortex DW is the lowest energy configuration in wide, thick structures. In the transverse DW the magnetization forms a V-shaped arrangement with the magnetization rotating in the plane of the wire, whereas the vortex DW is similar to the vortex state in disks and squares with the magnetization rotating around a central core region which is out-of-plane magnetized, as revealed by electron holography [60].

In addition to the rich range of physical phenomena that are revealed in these systems, the efficient and controlled manipulation of these quasi-particles is also the basis of a variety of proposed devices including sensors [61], data-storage concepts [62] and magnetic logic [63]. For such devices domain walls need first to be controllably nucleated and then carefully manipulated using either magnetic fields or currents and since the time-scale of operation of the devices is intricately linked to the fundamental dynamics of the system, fast-imaging techniques are often highly advantageous in order to understand the fundamental factors which limit speeds. In the following, insight gained from the magnetic imaging of these different stages of device operation will be outlined.

3.1. Fast Domain Wall Generation

Firstly domain walls need to be created. We here study the fast creation of two DWs in a permalloy nanowire (200 nm wide and 20 nm thick) that can be imaged when consecutive Oersted field pulses of alternating polarity are employed as shown in **Figure 8A** [64]. This way the magnetization underneath the field generating stripline is always antiparallel to the Oersted field. Two DWs are created with every pulse by reversal of the magnetization giving a black/white contrast in the X-ray micrographs (**Figure 8B**). The first pulse injects two walls into an initially uniformly magnetized wire, while the second pulse creates two walls that collide with the initial ones and annihilate each other. After the mutual annihilation the nanowire is again uniformly magnetized. To achieve a successful generation pulse lengths of a few nanoseconds are required [65, 66] and the whole process is repeatable at high frequencies for time-resolved imaging by an asynchronous excitation pump and probe scheme. **Figure 8C** shows the creation of two walls by a 6 ns long pulse. After 1.1 ns a vortex core emerges underneath the stripline followed by a second one at 1.7 ns. The vortices are separated by the 60 mT Oersted field. During the motion away from the stripline, the walls transform to transverse walls and back around 2.9 ns due to the high driving field being well above the Walker breakdown. Outside the stripline vicinity, the field strength decreases and the walls become pinned.

A similar measurement scheme can be applied for the observation of domain-wall motion in lower fields. **Figure 8D** shows a 2 μm wide stripline across a V-shaped 20 nm thick nanowire. By horizontal saturation with an external magnetic field vortex DWs can be created at the kink [67]. The wire widens in both directions away from the kink creating a potential well for the wall. Additionally the wall is pinned at the kink itself. Excitation of the wall by 2 ns and 3 ns long Oersted field pulses result in a damped oscillation of the wall at the pinned position or in depinned outwards motion. The depinned wall is pushed upwards and continues its motion for 2.7 ns after the pulse is over due to its inertia [68]. The potential from the widening wire then pushes the DW back to its initial position at the kink enabling a fast repetition of the motion for time-resolved imaging shown in **Figure 8E** [69]. The pulse compresses the wall and initiates oscillations of the wall width. During compression the wall accelerates and it reaches the turning point at the top when the maximum overexpansion occurs. An oscillation of the vortex core (transition from black to white in **Figure 8E**) around the averaged DW centre is also observed.

3.2. Field Induced Domain Wall Dynamics

To study continuous sustained motion at longer timescales, ferromagnetic nanoscale rings [70] are ideally suited as here domain walls can be driven around the perimeter of the ring multiple times [71]. Furthermore, rings have been of great interest due to their proposed application in sensory and memory devices [72–74]. Their suitability stems from the closed-flux state of the vortex configuration suggesting that magnetic nanorings could be packed densely without coupling with neighbors, and two-fold degeneracy of their circulation (clockwise versus counterclockwise) that might be used for coding of two logical values [71]. Good control of the ring circulation was reported for asymmetric rings by the use of in-plane magnetic fields with a particular direction with respect to the symmetric axis of asymmetric rings [58, 75], which provide for a good control of the logical value of proposed memory elements [76]. While most of these applications primarily exploit the static properties of the vortex configuration, dynamical switching and the propagation of DWs in curved nanowires has recently come to the center of interest due to the high complexity and richness of their dynamics [77]. Steady-state motion of ferromagnetic DW in straight wires is limited by the occurrence of a Walker breakdown, above which changes to a wall's internal spin structure take place, leading to intrinsically oscillating DW velocity. Such a behavior was

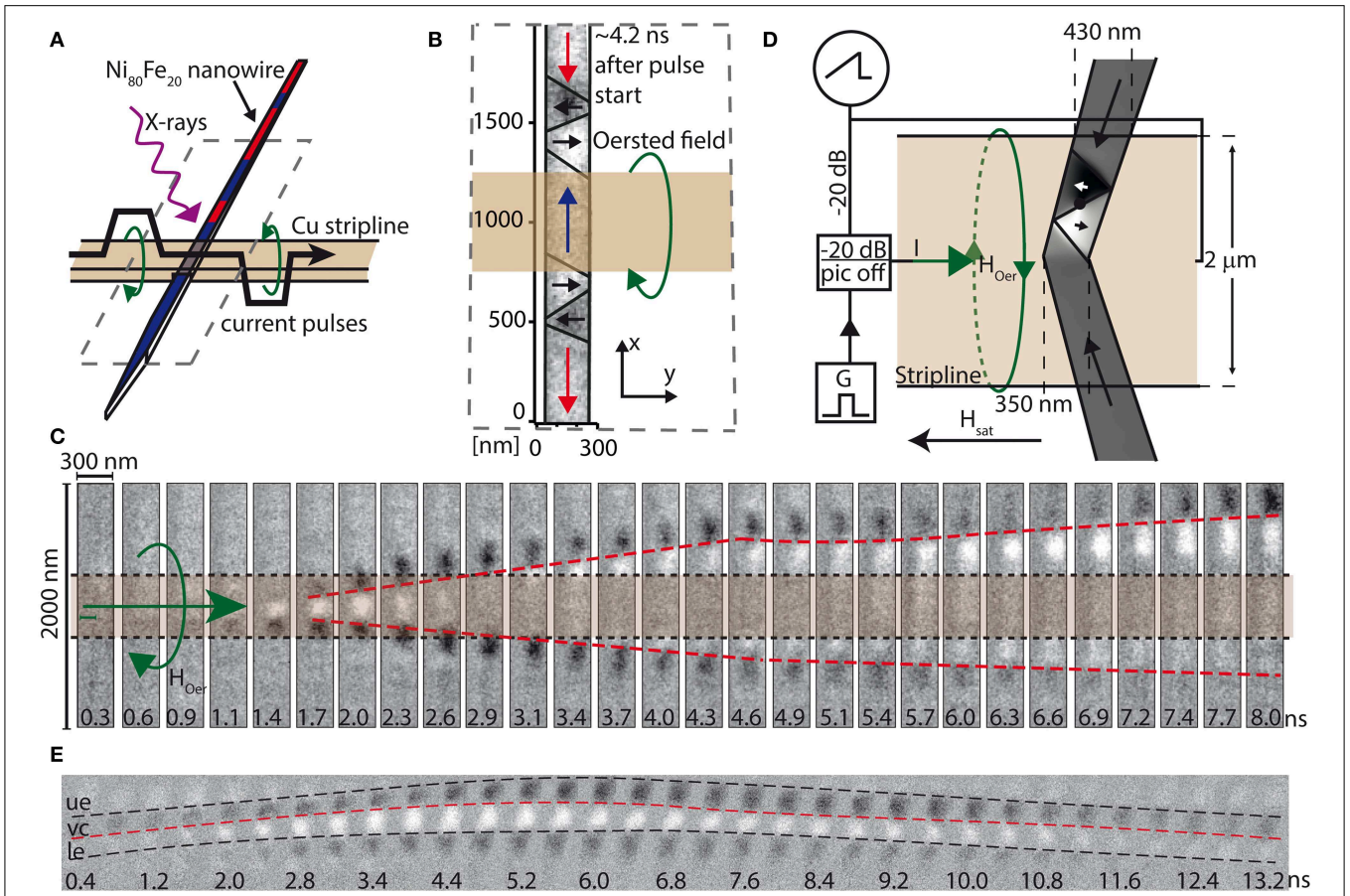

FIGURE 8 | (A) Measurement scheme for time-resolved imaging of the fast creation of domain walls (DWs) in a nanowire (red/blue) by Oersted field pulses (green) around a stripline (beige). The imaged area is depicted in **(B)** showing two vortex DWs with a black/white contrast. **(C)** Fast creation of two vortex DWs undergoing structural transformations by a 6 ns long 60 mT field pulse. **(D)** Scheme for low field motion imaging. The wall is injected by horizontal saturation of the V-shaped nanowire. The wire widens away from the kink creating an attractive potential. **(E)** A vortex DW is pushed upwards from the kink by a 3 ns long 3.6 mT field pulse and returns to its initial position due to the widening of the wire. The upper- and lower edge (ue and le, black dashed lines) are marked together with the vortex core position (red dashed line).

qualitatively firstly predicted by Walker [78]. He found out that a 180° DW in an infinite uniaxial magnetic medium, subjected to a uniform magnetic field, can move in two successive regimes: (i) a steady-state regime characterized by constant DW velocity (in a uniform DC field) followed by (ii) a regime of precessional motion, where internal spin structure changes take place, giving rise to oscillations in the velocity. Surprisingly, such behavior of DWs has been confirmed qualitatively in a wide range of magnetic materials differing by shape, dominant anisotropy [79, 80] and various driving mechanisms [81], even though the first theoretical predictions made by Walker do not contain boundary conditions defining the particular shape of wire. Such qualitative validity of the Walker solution far beyond its own limitation confirms the relevance of this model and good applicability. However, our recent research on DW dynamics of vortex DW in ferromagnetic rings shows strong deviations from this model. It is becoming apparent that the curvature of ferromagnetic ring gives rise to new phenomena in DW dynamics, which cannot be predicted within the simple one dimensional model. Direct visualization of vortex DW dynamics by STXM allows us to gain an insight into the problem, utilizing the advantage of a high temporal and space resolution on a micromagnetic scale. A distinctly different behavior of the vortex domain propagation below and above Walker breakdown is compared in a series of rings with different radii (**Figure 9**). For a smaller ring radius, the vortex core is pushed to the outer edge of the ring, but no transformation of the internal spin structure is observed, which suggests that the wall moves below Walker breakdown. On the other hand, the DW in a larger ring at a slightly higher average velocity experiences periodical transformation of wall structure from the vortex to the transverse one and vice versa. As is seen in the figure, not only the vortex core polarization, but also the circulation of the vortex DW is conserved in ferromagnetic rings, as opposed to straight wires, where both vortex core circulation and polarization alter during the Walker breakdown [57]. In addition, the curvature of ferromagnetic rings gives rise to the oscillatory motion of the vortex DW [77], which occurs even below Walker breakdown (**Figure 10**). This behavior cannot be

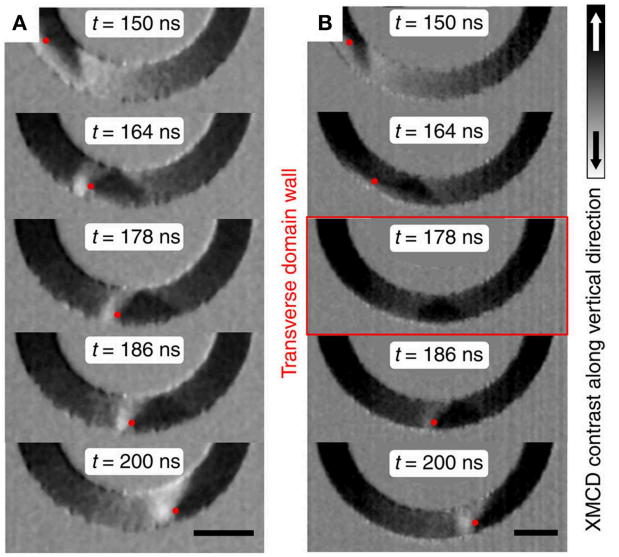

FIGURE 9 | From Bisig et al. [77]. Snapshots of vortex domain wall dynamics driven by 5 MHz counter-clockwise rotating field pulse in a ring of **(A)** 2.0 μm and **(B)** 2.5 μm radius.

the result of extrinsic pinning, since the position of the velocity maxima changes with the initial starting angle of the DW. The underlying mechanism of oscillatory motion can be explained by the forces that act on vortex core during the motion [77]. Assuming a non-zero phase shift ϕ (for zero phase shift, there is no force acting on the DW from external field, because of its position at the energy minimum), there are three significant forces: (i) the tangential component of the rotating field, $H_t = H \sin\phi$, acts in the radial and azimuthal direction, (ii) the gyroforce $G \times v$ acts solely in the radial direction (its orientation depends on the vortex polarization and sense of rotation in the ring) and finally (iii) the restoring force due to the shape anisotropy, which depends on the radial position of the vortex in the ring. The interplay between these forces can accelerate the DW so that it can overtake the driving field. During this process, the DW experiences energetically unfavorable motion toward the region of higher energy (characterized by negative phase shift), which highlights the important role of DW inertia for this (intrinsic oscillatory) behavior. On the other hand, variations of the local DW velocity are strongly influenced by pinning centers and imperfections of the material as well. Extrinsic pinning modulates the local potential landscape of the DW and the resulting interplay between intrinsic and extrinsic pinning is additionally obscured by stochastic processes.

3.3. Synchronous Field Driven Motion of Magnetic Domain Walls

Whilst field driven motion is a well established, efficient way of achieving fast DW motion, it is often thought to be incompatible with devices such as the Racetrack memory where multiple domain walls need to be synchronously propagated along a magnetic wire [62]. This is because when a field is applied along the same axis as the magnetization, the Zeeman energy contribution makes it favorable for domains which are aligned with the field to grow in size at the expense of those which are anti-aligned with the field. In the case of a single domain wall in a nanowire, this can indeed lead to DW propagation, however when there are multiple DWs in the nanowire the change in magnetization direction across successive DWs necessarily alternates (between head-to-head and tail-to-tail in the case of in-plane magnetized systems), which means that neighboring DWs move in opposite directions and ultimately the domains collapse [82]. Recently, however, Kim et al. have demonstrated a scheme whereby in-plane magnetized transverse walls of fixed circulation can be synchronously displaced using out-of-plane field pulses [83]. During the application of an out-of-plane field pulse, the magnetization in the DW begins to precess around the field direction, leading to a displacement of the DW along the wire. At the same time, however, the magnetization is damped into the field direction, leading to a demagnetizing field that eventually stops the motion. For symmetric pulses, the DW will move back to its initial position on relaxation when the field is turned off, however, since the force on the wall depends on the rate-of-change of the excitation [84] the forward and backward forces can be tailored by employing asymmetric pulses. If, furthermore, preferential pinning sites are provided by tailoring the geometry of the system, a net displacement of the DW can indeed be achieved. From a one-dimensional analytical model of the system it is revealed that the direction of this displacement is correlated to the direction of the field and the circulation of the DW [83], so by having a fixed circulation of DWs synchronous motion of multiple DWs can be achieved, even when the DWs alternate between head-to-head and tail-to-tail configurations. Note that here we talk about the circulation of a transverse wall, which is distinctly different from the circulation definition for vortex walls. In addition to the analytical model, the scheme is further demonstrated in a device relevant geometry using micromagnetic simulations. Experimental demonstration of the effect was provided by STXM imaging of DW displacement in Permalloy half rings. Asymmetric current pulses, typically of 700 ps rise time, 5 ns width and 1100 ps fall time, were applied to a gold strip-line located beside the wires in order to generate the asymmetric out-of-plane field. The corresponding displacement of the DWs was observed and found to be in perfect agreement with the expected directional displacement as a function of the circulation of the wall and the direction of the field. Also for a single DW, reversing the direction of the field pulse led to the expected reversal of DW displacement direction. Furthermore, the calculated efficiency of the experimental displacement was found to compare favorably with alternative approaches of DW propagation.

3.4. Current Induced Domain Wall Dynamics

An alternative approach to domain wall motion is current induced DW motion (CIDWM) which can also provide synchronous motion of multiple DWs. While it exhibits good scaling, one drawback of CIDWM is the high-critical current densities required for many of the conventional STT driven effects, which can be problematic due, for instance, to Joule heating [85, 86], which can be partly remedied by thermal cooling

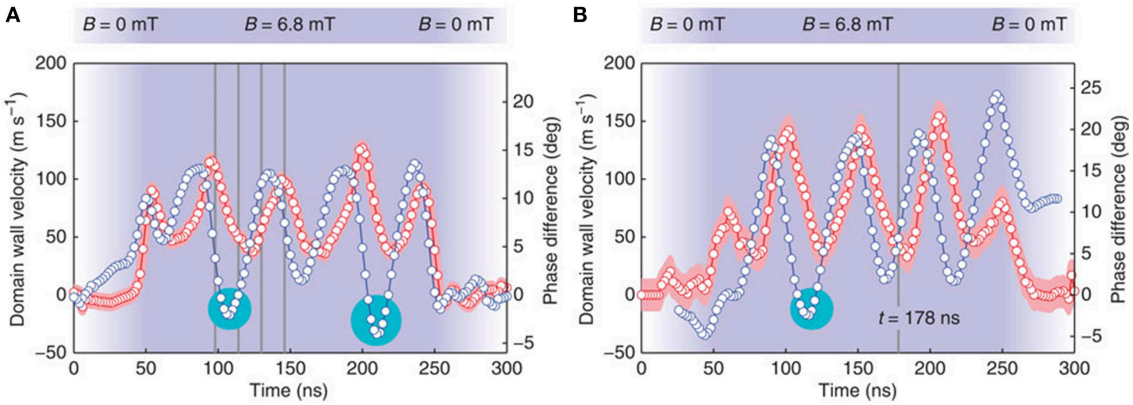

FIGURE 10 | From Bisig et al. [77]. Time dependence of domain wall velocity and phase shift for the DW motion **(A)** below and **(B)** above Walker breakdown in a ferromagnetic ring.

layers [87]. For CIDWM induced by conventional spin transfer torque (STT) the dynamics of the system can be described by the phenomenological Landau-Lifschitz-Gilbert equation:

$$\frac{\partial \vec{m}}{\partial t} = \gamma \mu_0 \vec{H} \times \vec{m} + \alpha \vec{m} \times \frac{\partial \vec{m}}{\partial t} - (\vec{u} \cdot \vec{\nabla})\vec{m} + \beta[\vec{m} \times (\vec{u} \cdot \vec{\nabla})\vec{m}], \quad (3)$$

where $\gamma = g|\mu_B|/\hbar$ is the gyromagnetic ratio which governs the precession of the magnetization around the effective field and α is the Gilbert parameter which quantifies the damping of the system [88, 89]. The last two terms incorporate the effect of the current by way of the adiabatic and non-adiabatic torques, respectively [90, 91]. Here $\vec{u} = \vec{J}Pg\mu_B/2eM_s$ is the so-called spin drift velocity and β is the non-adiabaticity of the current flow. Different contributions for the non-adiabatic torque have been identified, including spin-relaxation due to spin-flip scattering at, e.g., impurities or phonons [90–96] and a pure non-adiabatic contribution due to the mistracking of the conduction electron spins with the local magnetization [93, 94, 96, 97], which becomes more important for large magnetization gradients -i.e., at narrow DWs or at vortex cores. For CIDWM, the degree of this non-adiabaticity of the electron transport through the domain wall and the ratio of β to α are key factors which determine the details of the dynamics of the system and correspondingly important device parameters such as the DW velocity [55, 90, 94, 98–103].

One class of measurements that can be performed in order to extract important dynamic parameters of the system are quasi-static measurements whereby the DW is imaged before and after the application of current pulses to the wire. This yields the average DW velocity from the net displacement of the wall and with suitably high-resolution imaging changes in spin-structure can also be determined [104–108]. The measured DW velocity is not only related to the spin structure and the intrinsic material parameters of the system, but also to the pinning potential landscape and the details of the excitation pulse. It turns out that the force on a DW is strongly related to the time derivative of the current pulse, with fast changing current pulses exerting much larger forces than constant currents [84]. As a result, short rise-time pulses are observed to lead to much larger DW velocities since the wall is able to overcome local pinning sites before the imparted energy is dissipated to damping [109]. For ultra-short pulses with a rise time of around 100 ps or less, very fast STT driven DW motion above 100 m/s has been observed even for in-plane magnetized Permalloy [105, 108]. This is shown in **Figure 11**. The initial configuration is shown in the top of the XMCD-PEEM image of **Figure 11A**, with the contrast showing good agreement with that expected from a micromagnetic simulation of a vortex DW, as shown below the wires. Successively, following the injection of single current pulses, the change in the spin-configuration is measured as displayed in the following images (from top to bottom). **Figure 11B** presents line scans showing the displacement and the transformation of the DW. Whilst the right side continuously moves in the direction of the electron flow, after the third current pulse the left side seems to become pinned and no longer moves. The DW is therefore stretched, which results in an increase of the stray field energy. Eventually this becomes larger than the energy required for a vortex core nucleation and at this point it is energetically more favorable to transform to an antiparallel double vortex wall by vortex core nucleation. The new DW structure then displaces under current injection similar to before, without further changes to its spin structure. From the average displacement per current pulse of 400 nm and the measured pulse length of 3 ns this results in an average DW velocity of 130 m/s, which is much larger than for long currents pulses (>10 μs).

The imaging can also reveal key information about the size of the two STT terms. For transverse walls, up to a certain point, the so-called Walker breakdown, the average DW velocity, $\langle v \rangle$, is proportional to the current-density and expected to depend on the ratio of β and α up to a critical velocity: $\langle v \rangle = \frac{\beta}{\alpha} u$ [90, 91, 94, 102]. The threshold current density for Walker breakdown depends on the difference between β and α [91, 98, 101]. In the case that $\beta = \alpha$ the Walker breakdown is suppressed and the DW always propagates without distortion. Conversely, if $\beta \neq \alpha$ then the DW spin structure is expected to oscillate, leading to either a reduction or an increase in the average velocity depending on whether β is greater or less than α, respectively. Finally, for very large current density the final DW velocity approaches

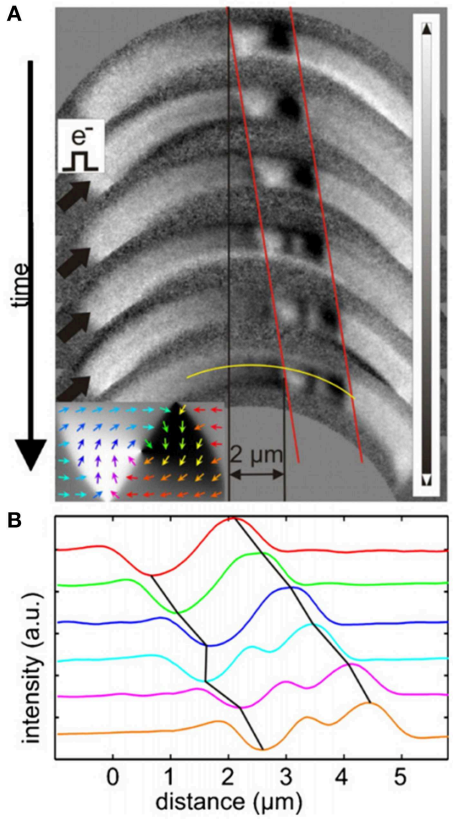

FIGURE 11 | From Heyne et al. [108] (A) Photoemission electron microscopy image series of a Py wire (1000 nm wide, 40 nm thick with a 2 nm Au capping) containing a vortex DW. The top image shows the configuration after the initialization by a short vertical field pulse. The inset in the lower left shows a micromagnetic simulation of a VW to help visualize the DW structure. The XPEEM images were taken with vertical contrast (see grayscale bar at the right) and the simulation was adapted to this contrast. Current pulses were injected between adjacent images (from top to bottom). After five injections the DW is displaced by 2 Î¼m, thus about 400 nm on average per current pulse. After the third pulse DW transformed to a double vortex that continues moving. **(B)** Intensity line scans along the yellow curve indicated by the yellow line in **(A)**.

$\langle v \rangle = \frac{1+\alpha\beta}{1+\alpha^2} u$. Heyne et al. experimentally imaged the spin structure on current injection [104, 106] using XMCD-PEEM (the setup is described in Heyne et al. [110]), revealing that at high current densities periodic transformations of the DW between vortex and transverse can occur which can be attributed to STT as opposed to defects, directly indicating that $\beta \neq \alpha$ in this case. Similarly Meier et al. imaged current driven distortions of double vortex-wall structures using magnetic transmission X-ray microscopy and from the size of the displacement extracted an estimate for β/α. Moore et al. went further by looking at the scaling between β and α. The damping was engineered in the Permalloy films by rare earth doping with Ho [111] and the DW velocity determined from XMCD-PEEM images, as above, as a function of the current density in order to determine the point of Walker breakdown [107]. It was found that up to 4% Ho doping the two parameters scaled with each other, in agreement with theories which predict that the angular momentum dissipation which causes the damping and the spin relaxation that leads to the nonadiabatic transport have a similar origin [95, 112].

As for vortex DWs, the core region of vortices in squares/discs is also displaced on the application of current pulses to the system [106]. A measurement scheme for extracting the different contributions from adiabatic and non-adiabatic torques to this motion was proposed by Krüger et al. [113] based on imaging the steady-state vortex core displacement resulting from the application of a current. Since the adiabatic and non-adiabatic torques act perpendicularly to each other, leading to displacement either perpendicular to or along the current flow direction, respectively, the relative contributions can be extracted and separated from Oersted field effects by measuring the direction and magnitude of displacement for different configurations of the vortex state polarization and circulation. Heyne et al. implemented this scheme using XMCD-PEEM to image the vortex core displacement in Permalloy discs [114]. The resulting non-adiabaticity was found to be $\beta = 0.15 \pm 0.07 > 10\alpha$. Such a high value can be correlated with the vortex core region of the structure, demonstrating a significant contribution from non-adiabatic transport in systems with a high magnetization gradient . A similar experiment has recently also been carried out in Permalloy squares using scanning electron microscopy with polarization analysis for the magnetic imaging, with β found to be 0.119 ± 0.022 [115], in good agreement with the photon-based imaging.

Finally, dynamic magnetic imaging has also been applied in order to quantify the effect of the magnetization gradient in the DW on the behavior, which should also contribute to the pure non-adiabatic component of β. Eltschka et al. have used transmission electron microscopy to image the thermally activated hopping of DWs between two pinning sites in Permalloy [116], with the Fresnel mode of Lorentz microscopy [117] employed in order to dynamically track the position of the wall and off-axis electron holography [118] providing detailed maps of the spin structure and magnetization gradient. The dwell times of the DW in the two pinning sites, which can be described by an Arrhenius law [92], are measured as a function of the current density applied to the wire. The non-adiabatic torque acts as a force on the DW, modifying the potential landscape and in turn changing the ratio of the two dwell times and from the observed dependency β can be extracted. Very different values are found for transverse and vortex DWs. In the former case a value of $\beta = 0.010 \pm 0.04 \approx 1.3\alpha$ whereas a much larger value is found for the latter case with $\beta = 0.073 \pm 0.026 \approx 9.2\alpha$. This can again be attributed to the large magnetization gradient at the vortex core, implying a clear pure non-adiabatic contribution to the non-adiabaticity in this case.

Another key consideration of current driven magnetization dynamics is the influence of the pinning potential, since this can strongly influence the dynamics and DW velocities, depending also on the rise-time of the current excitations [84]. The pinning of vortices and vortex DWs can be studied through dynamic imaging of the alternating current (ac) driven excitation of vortex core gyration [119, 120]. Bolte et al. used STXM in order to image the time-resolved gyration of the vortex core in a Permalloy square which was excited by both fields and STT. The sense of rotation of the vortex core gyration is set by the polarization

of the vortex core, meanwhile the phase of the motion depends on the circulation of the state for field driven motion yet is independent of the circulation in the case of STT driven excitation [53, 121, 122]. The observed vortex gyration due to ac fields or currents can be described by a rigid core within a two-dimensional harmonic oscillator potential [121]. By comparing the observed current driven motion to that predicted by the model, the separate contributions of the Oersted field and STT to the dynamics could be extracted by comparing states with opposite circulation, since only the field driven component of the excitation is changed. Bisig et al. used a similar methodology to investigate the gyration of a vortex domain wall pinned beside a constriction in a Permalloy wire [120]. Here the situation is more complicated since the potential well is asymmetric and the vortex core has a varying velocity depending on its position. Conversely, the nanowire geometry allows a spatial separation of the contacts and the pinned wall, minimizing the influence of Oersted fields. In the work the gyrotropic motion of the vortex core is imaged as a function of the excitation frequency and the displacement and phase of the oscillations are extracted. The trajectory of the core at 340 MHz, near the resonant frequency of 334 ± 12 MHz, is observed to have a noticeable eccentricity of $e = 0.77 \pm 0.04$ and a tilt angle of $\theta = 10.1 \pm 0.5\ ^\circ$ with respect to the notch, confirming the asymmetry of the pinning potential. Furthermore, from the analytical model of a two-dimensional harmonic oscillator potential [121] the stiffness of the local potential could be calculated.

4. Dynamics of Magnetic Bubbles

Magnetic vortices exist in materials with in-plane anisotropy. Their counterparts in systems with a strong out-of-plane easy axis are called magnetic bubbles, which are skyrmionic spin structures as they exhibit the topology with a non-trivial skyrmion winding number [123]. Inside the bubble the magnetization points perpendicular to the film plane. In the region outside the bubble the magnetization points in the opposite direction. Both regions are separated by a Bloch type DW in which the magnetization curls in-plane around the center of the bubble.

The bubble skyrmion exhibits dynamics that are different compared to a vortex. While a free vortex gyrates on a spiral trajectory, the bubble moves on a hypocyclodic trajectory [124]. The displacement and deformations of a bubble skyrmion can be readily understood by waves that travel along the DW that confines the bubble skyrmion [125]. For each wave number k there are two waves that travel in opposite directions with different speeds. The modes with $k = 1$, that is the wave length is exactly the circumference of the bubble, turn out to be equal to a displacement of the bubble skyrmion. These two modes yield an equation of motion of [125]:

$$-M\ddot{\mathbf{R}} + \mathbf{G} \times \dot{\mathbf{R}} - D\dot{\mathbf{R}} - K\mathbf{R} = 0, \tag{4}$$

where $\mathbf{R}$ is the center of the bubble and $-K\mathbf{R}$ is the confining force of a harmonic potential. $\mathbf{G}$ and D are the gyro vector and dissipation tensor, respectively [53, 126]. In addition to the Thiele equation that is known to describe the displacement of a magnetic vortex, Equation (4) contains some inertia that is described by the mass M.

Neglecting the damping, that is $D = 0$, Equation 4 has two circular eigenmodes with the frequencies

$$\omega_\pm = \frac{G_z}{2M} \pm \sqrt{\left(\frac{G_z}{2M}\right)^2 + \frac{K}{M}}. \tag{5}$$

In the limit of $M \to 0$, as for the vortex, the high frequency mode in Equation (5) goes to infinity while the low frequency mode becomes K/G as known from a vortex.

X-ray holography [127] has recently been used to study the dynamics of such systems. The advantage of this technique is that it is drift free allowing a measurement of the bubble position with a high accuracy. In the experiment [123, 128, 129] a multilayer film of CoB/Pt has been grown on a thin SiN membrane to allow the photons to be transmitted through the sample. The magnetic layer, that is CoB, is amorphous, reducing the pinning compared to the pinning at crystalline imperfections in a pure Co film. The CoB/Pt film is patterned to a disc element. This element is surrounded by a gold microcoil as shown in **Figure 12A**. The system is then excited by sending the current pulse shown in **Figure 12B** through the microcoil. The Oersted field then excites the magnetic structure. As can be seen in **Figure 12A** there are two bubble skyrmions, however, one of them turns out to be pinned. After the current pulse the bubble skyrmion performs a motion on a hypocyclodic trajectory. A part of this trajectory is shown in **Figure 12**. From the shape of the trajectory the skyrmion number is deduced to be 1 and we extract the effective mass [123].

5. Summary

In summary we have presented an overview of the dynamics of confined spin structures. From the dynamic imaging using X-ray based techniques, we have deduced the underlying physics of the dynamics that is found to depend on the material, geometry and excitation method. The discovery of vortex core reversal by the creation of a vortex-antivortex pair triggered a new chapter in vortex dynamics. Milestones are the excitation of the (sub-GHz) vortex gyromode by ac magnetic fields or electrical currents, unidirectional vortex core switching by rotating magnetic fields and the excitation of (multi-GHz) azimuthal spin waves which allows speeding up of vortex core reversal to less than 100 ps. The concept of coupled harmonic oscillators is applicable to a system of coupled magnetic vortices. By self-organized state formation it is possible to write distinct polarization configurations. Eigenmodes of such artificial crystals can be tuned at will, paving the way to customizable band structures in magnonic vortex crystals. Processes to consecutively create domain walls to obtain multiple walls inside one wire or to mutually annihilate the walls are demonstrated. The time structure of the creation process is analyzed by transmission X-ray microscopy in combination with micromagnetic simulations. After wall formation transformations are directly observed above a critical driving field, the Walker breakdown. Internal excitations of vortex domain walls

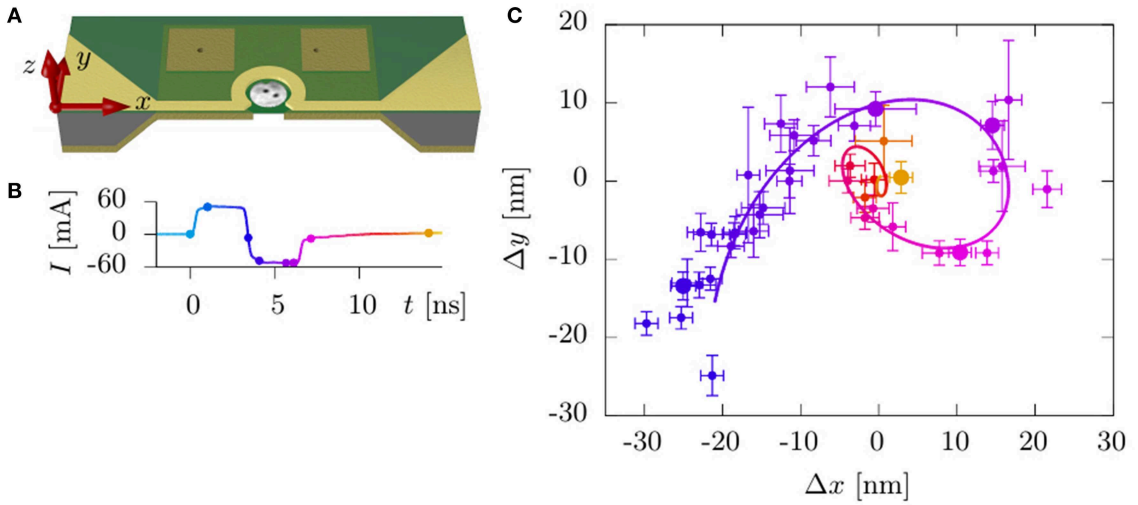

FIGURE 12 | Partly from Büttner et al. [123]. (A) Schematic depiction of the experimental setup. The CoB/Pt disc is surrounded by a gold stripline that generates a field. **(B)** The shape of the bipolar current pulse. **(C)** Measured positions of the bubble as a function of time [color code depicts the time and is the same as in **(B)**]. The line is a fit with Equation (4) to extract the skyrmion properties.

are also found in low field motion. A strong interplay between internal dynamics and the macroscopic motion is identified. The dynamics of domain walls in curved geometries shows a universal oscillation of the velocity, which can be understood from the interplay of the acting torques on the wall. Furthermore, multiple domain walls can be driven synchronously by choosing a perpendicular field geometry when combined with specially tailored pinning sites and field pulse shapes. Current-induced wall motion can naturally lead to synchronous wall motion as required for devices. Fast wall motion is observed for short pulses and the efficient displacement of vortex walls can be attributed to the large non-adiabaticity, which is corroborated by measurements on vortex cores. Beyond domain walls, more complex quasi-particles are skyrmions that exhibit complex dynamics. For bubble skyrmions that are non-chiral, the spiralling trajectory results from the interplay of two waves with different frequencies from which a large effective mass results. All this can only be directly evaluated using high resolution x-ray based dynamic imaging. The broad applicability of the imaging bodes well for future investigations using novel dynamic imaging techniques for instance at light sources that provide shorter time scales such as Free Electron Lasers.

Acknowledgments

We would like to thank Michael Bechtel and Iuliia Bykova at the MPI MAXYMUS endstation at BESSY II, Berlin, as well as the BESSY staff for their continuous support and the HZB for the allocation of synchrotron radiation beamtime. We also are grateful to Bartel Van Waeyenberge for the long lasting cooperation in implementing time-resolved measurements at scanning transmission X-ray microscopes. The group from Stuttgart would like to thank Manfred Fähnle and Christian H. Back for many fruitful discussions, Ajay Gangwar and Georg Woltersdorf for the preparation of the samples and Ulrike Eigenthaler for SEM imaging. We are indebted to many PhD students and postdocs, in particular Aleksandar Puzic, Kang Wei Chou, Michael Curcic, Matthias Kammerer, Markus Sproll, and Georg Dieterle; our results would not have been possible without the work of all of them. The group from Hamburg would like to thank Ulrich Merkt for discussions, encouragement and continuous support and Michael Volkmann for superb technical assistance. Financial support by the Deutsche Forschungsgemeinschaft (DFG) through the Sonderforschungsbereich 668, the Graduiertenkolleg 1286 and the Hamburg Centre for Ultrafast Imaging (CUI) is gratefully acknowledged. The group from Mainz is indebted to a number of students, postdocs and colleagues which have contributed to these experiments and calculations. Parts of this work were performed within the EU projects MAGWIRE (FP7-ICT-2009-5 257707), WALL (FP7-PEOPLE-2013-ITN 608031) the European Research Council Starting Independent Researcher Grant MASPIC (No. ERC-2007-StG 208162) and furthermore the Graduate School of Excellence "Materials Science in Mainz" (No. GSC266). We acknowledge the Deutsche Forschungsgemeinschaft (DFG) and the State Research Center of Innovative and Emerging Materials at Johannes Gutenberg University for financial support. Some of the figures in this paper have been modified from figures of our own publications.

References

1. Hubert A, Schäfer R. *Magnetic Domains: The Analysis of Magnetic Microstructures.* Berlin; Heidelberg: Springer-Verlag (1998).
2. Kläui M, Vaz CAF. *Handbook of Magnetism and Advanced Magnetic Materials,* Vol. 2, Chichester: John Wiley and Sons (2007).
3. Kammerer M, Weigand M, Curcic M, Noske M, Sproll M, Vansteenkiste A, et al. Magnetic vortex core reversal by excitation

of spin waves. *Nat Commun.* (2011) **2**:279. doi: 10.1038/ncomms 1277

4. Kammerer M. *Spinwelleninduziertes Schalten Magnetischer Vortexkerne.* PhD thesis, Stuttgart: University of Stuttgart (2011).
5. Stöhr J, Wu Y, Hermsmeier BD, Samant MG, Harp GR, Koranda S, et al. Element-specific magnetic microscopy with circularly polarized X-rays. *Science* (1993) **259**:658–61.
6. Quitmann C, Raabe J, Buehler C, Buess M, Johnson S, Nolting F, et al. Measuring magnetic excitations in microstructures using X-ray microscopy. *Nucl Instrum Methods Phys Res A* (2008) **588**:494–501. doi: 10.1016/j.nima.2008.01.093
7. Van Waeyenberge B, Puzic A, Stoll H, Chou KW, Tyliszczak T, Hertel R, et al. Magnetic vortex core reversal by excitation with short bursts of an alternating field. *Nature* (2006) **444**:461–4. doi: 10.1038/nature05240
8. Raabe J, Pulwey R, Sattler R, Schweinbock T, Zweck J, Weiss D. Magnetization pattern of ferromagnetic nanodisks. *J Appl Phys.* (2000) **88**:4437–9. doi: 10.1063/1.1289216
9. Shinjo T, Okuno T, Hassdorf R, Shigeto K, Ono T. Magnetic vortex core observation in circular dots of permalloy. *Science* (2000) **289**:930–2. doi: 10.1126/science.289.5481.930
10. Ross C, Hwang M, Shima M, Cheng J, Farhoud M, Savas T, et al. Micromagnetic behavior of electrodeposited cylinder arrays. *Phys Rev B* (2002) **65**:144417. doi: 10.1103/PhysRevB.65.144417
11. Feldtkeller E, Thomas H. Struktur und Energie von Blochlinien in dünnen ferromagnetischen Schichten. *Phys Kondens Mater* (1965) **4**:8–14.
12. Miltat J, Thiaville A. Vortex cores - Smaller than small [Editorial Material]. *Science* (2002) **298**:555. doi: 10.1126/science.1077704
13. Wachowiak A, Wiebe J, Bode M, Pietzsch O, Morgenstern M, Wiesendanger R. Direct observation of internal spin structure of magnetic vortex cores. *Science* (2002) **298**:577–80. doi: 10.1126/science.1075302
14. Choe SB, Acremann Y, Scholl A, Bauer A, Doran A, Stöhr J, et al. Vortex core-driven magnetization dynamics. *Science* (2004) **304**:420–2. doi: 10.1126/science.1095068
15. Cheng XM, Buchanan KS, Divan R, Guslienko KY, Keavney DJ. Nonlinear vortex dynamics and transient domains in ferromagnetic disks. *Phys Rev B* (2009) **79**:172411. doi: 10.1103/PhysRevB.79.172411
16. Okuno T, Shigeto K, Ono T, Mibu K, Shinjo T. MFM study of magnetic vortex cores in circular permalloy dots: behavior in external field. *J Magn Magn Mater.* (2002) **240**:1–6. doi: 10.1016/S0304-8853(01) 00708-9
17. Thiaville A, García JM, Dittrich R, Miltat J, Schrefl T. Micromagnetic study of Bloch-point-mediated vortex core reversal . *Phys Rev B* (2003) **67**:094410. doi: 10.1103/PhysRevB.67.094410
18. Vansteenkiste A, Chou KW, Weigand M, Curcic M, Sackmann V, Stoll H, et al. X-ray imaging of the dynamic magnetic vortex core deformation . *Nat Phys.* (2009) **5**:332–4. doi: 10.1038/nphys1231
19. Hertel R, Gliga S, Fähnle M, Schneider CM. Ultrafast nanomagnetic toggle switching of vortex cores. *Phys Rev Lett.* (2007) **98**:117201. doi: 10.1103/PhysRevLett.98.117201
20. Xiao QF, Rudge J, Choi BC, Hong YK, Donohoe G. Dynamics of vortex core switching in ferromagnetic nanodisks. *Appl Phys Lett.* (2006) **89**:262507. doi: 10.1063/1.2424673
21. Kim SK, Choi YS, Lee KS, Guslienko KY, Jeong DE. Electric-current-driven vortex-core reversal in soft magnetic nanodots. *Appl Phys Lett.* (2007) **91**:082506. doi: 10.1063/1.2773748
22. Lee KS, Guslienko KY, Lee JY, Kim SK. Ultrafast vortex-core reversal dynamics in ferromagnetic nanodots. *Phys Rev B* (2007) **76**:174410. doi: 10.1103/PhysRevB.76.174410
23. Guslienko KY, Lee KS, Kim SK. Dynamic origin of vortex core switching in soft magnetic nanodots. *Phys Rev Lett.* (2008) **100**:027203. doi: 10.1103/PhysRevLett.100.027203
24. Weigand M, Van Waeyenberge B, Vansteenkiste A, Curcic M, Sackmann V, Stoll H, et al. Vortex core switching by coherent excitation with single in-plane magnetic field pulses. *Phys Rev Lett.* (2009) **102**:077201. doi: 10.1103/PhysRevLett.102.077201
25. Yamada K, Kasai S, Nakatani Y, Kobayashi K, Kohno H, Thiaville A, et al. Electrical switching of the vortex core in a magnetic disk. *Nat Mater.* (2007) **6**:269–73. doi: 10.1038/nmat1867
26. Yamada K, Kasai S, Nakatani K Yoshinobu Kobayashi, Ono T. Switching magnetic vortex core by a single nanosecond current pulse. *Appl Phys Lett.* (2008) **93**:152502. doi: 10.1063/1.3001588
27. Curcic M, Van Waeyenberge B, Vansteenkiste A, Weigand M, Sackmann V, Stoll H, et al. Polarization selective magnetic vortex dynamics and core reversal in rotating magnetic fields. *Phys Rev Lett.* (2008) **101**:197204. doi: 10.1103/PhysRevLett.101.197204
28. Curcic M, Stoll H, Weigand M, Sackmann V, Juellig P, Kammerer M, et al. Magnetic vortex core reversal by rotating magnetic fields generated on micrometer length scales. *Phys Status Solidi B* (2011) **246**:2317–22. doi: 10.1002/pssb.201147208
29. Kamionka T, Martens M, Chou KW, Curcic M, Drews A, Schütz G, et al. Magnetic antivortex-core reversal by circular-rotational spin currents. *Phys Rev Lett.* (2010) **105**:137204. doi: 10.1103/PhysRevLett.105.137204
30. Kamionka T, Martens M, Chou KW, Drews A, Tyliszczak T, Stoll H, et al. Magnetic antivortex-core reversal by rotating magnetic fields. *Phys Rev B* (2011) **83**:224422. doi: 10.1103/PhysRevB.83.224422
31. Uhlir V, Urbanek M, Hladik L, Spousta J, Im MY, Fischer P, et al. Dynamic switching of the spin circulation in tapered magnetic nanodisks. *Nat Nanotechnol.* (2013) **8**:341–6. doi: 10.1038/nnano.2013.66
32. Kammerer M, Stoll H, Noske M, Sproll M, Weigand M, Illg C, et al. Fast spin-wave-mediated magnetic vortex core reversal. *Phys Rev B* (2012) **86**:134426. doi: 10.1103/PhysRevB.86.134426
33. Kammerer M, Sproll M, Stoll H, Noske M, Weigand M, Illg C, et al. Delayed magnetic vortex core reversal. *Appl Phys Lett.* (2013) **102**:012404. doi: 10.1063/1.4773592
34. Noske M, Gangwar A, Stoll H, Kammerer M, Sproll M, Dieterle G, et al. Unidirectional sub-100-ps magnetic vortex core reversal. *Phys Rev B* (2014) **90**:104415. doi: 10.1103/PhysRevB.90.104415
35. Donahue M, Porter D. *Oommf User's Guide, Version 1.0. Interagency Report NISTIR 6376.* Gaithersburg, MD: National Institute of Standards and Technology (1999).
36. Kruglyak VV, Demokritov SO, Grundler D. Magnonics. *J Phys D Appl Phys.* (2010) **43**:264001. doi: 10.1088/0022-3727/43/26/264001
37. Lenk B, Ulrichs H, Garbs F, Münzenberg M. The building blocks of magnonics. *Phys Rep.* (2011) **507**:107–36. doi: 10.1016/j.physrep.2011.06.003
38. Hänze M, Adolff CF, Weigand M, Meier G. Tunable eigenmodes of coupled magnetic vortex oscillators. *Appl Phys Lett.* (2014) **104**:182405. doi: 10.1063/1.4875618
39. Jung H, Yu YS, Lee KS, Im MY, Fischer P, Bocklage L, et al. Observation of coupled vortex gyrations by 70-ps-time- and 20-nm-space-resolved full-field magnetic transmission soft x-ray microscopy. *Appl Phys Lett.* (2010) **97**:222502. doi: 10.1063/1.3517496
40. Wang X, Keavney DJ, Asmat-Uceda M, Buchanan KS, Melikyan A, Cheng XM. Time-resolved photoemission electron microscopy imaging of mode coupling between three interacting magnetic vortices. *Appl Phys Lett.* (2014) **105**:102408. doi: 10.1063/1.4895070
41. Vogel A, Drews A, Kamionka T, Bolte M, Meier G. Influence of dipolar interaction on vortex dynamics in arrays of ferromagnetic disks. *Phys Rev Lett.* (2010) **105**:037201. doi: 10.1103/PhysRevLett.105.037201
42. Mejía-López J, Altbir D, Romero AH, Batlle X, Roshchin IV, Li CP, et al. Vortex state and effect of anisotropy in sub-100-nm magnetic nanodots. *J Appl Phys.* (2006) **100**:104319. doi: 10.1063/1.2364599
43. Sugimoto S, Fukuma Y, Kasai S, Kimura T, Barman A, Otani Y. Dynamics of coupled vortices in a pair of ferromagnetic disks. *Phys Rev Lett.* (2011) **106**:197203. doi: 10.1103/PhysRevLett.106.197203
44. Vogel A, Kamionka T, Martens M, Drews A, Chou KW, Tyliszczak T, et al. Coupled vortex oscillations in spatially separated permalloy squares. *Phys Rev Lett.* (2011) **106**:137201. doi: 10.1103/PhysRevLett.106.137201
45. Vogel A, Drews A, Weigand M, Meier G. Direct imaging of phase relation in a pair of coupled vortex oscillators. *AIP Adv.* (2012) **2**:042180. doi: 10.1063/1.4771683
46. Han DS, Vogel A, Jung H, Lee KS, Weigand M, Stoll H, et al. Wave modes of collective vortex gyration in dipolar-coupled-dot-array magnonic crystals. *Sci Rep.* (2013) **3**:2262. doi: 10.1038/srep02262

47. Shibata J, Otani Y. Magnetic vortex dynamics in a two-dimensional square lattice of ferromagnetic nanodisks. *Phys Rev B* (2004) **70**:012404. doi: 10.1103/PhysRevB.70.012404
48. Vogel A, Hänze M, Drews A, Meier G. Artificial band structure in anisotropic magnetic vortex crystals. *Phys Rev B* (2014) **89**:104403. doi: 10.1103/PhysRevB.89.104403
49. Shibata J, Shigeto K, Otani Y. Dynamics of magnetostatically coupled vortices in magnetic nanodisks. *Phys Rev B* (2003) **67**:224404. doi: 10.1103/PhysRevB.67.224404
50. Barman A, Barman S, Kimura T, Fukuma Y, Otani Y. Gyration mode splitting in magnetostatically coupled magnetic vortices in an array. *J Phys D Appl Phys*. (2010) **43**:422001. doi: 10.1088/0022-3727/43/42/422001
51. Adolff CF, Hänze M, Vogel A, Weigand M, Martens M, Meier G. Self-organized state formation in magnonic vortex crystals. *Phys Rev B* (2013) **88**:224425. doi: 10.1103/PhysRevB.88.224425
52. Krüger B, Drews A, Bolte M, Merkt U, Pfannkuche D, Meier G. Harmonic oscillator model for current- and field-driven magnetic vortices. *Phys Rev B* (2007) **76**:224426. doi: 10.1103/PhysRevB.76.224426
53. Thiele AA. Steady-state motion of magnetic domains. *Phys Rev Lett*. (1973) **30**:230. doi: 10.1103/PhysRevLett.30.230
54. Martens M, Kamionka T, Weigand M, Stoll H, Tyliszczak T, Meier G. Phase diagram for magnetic vortex core switching studied by ferromagnetic absorption spectroscopy and time-resolved transmission x-ray microscopy. *Phys Rev B* (2013) **87**:054426. doi: 10.1103/PhysRevB.87.054426
55. Boulle O, Malinowski G, Kläui M. Current-induced domain wall motion in nanoscale ferromagnetic elements. *Mater Sci Eng R Rep*. (2011) **72**:159–87. doi: 10.1016/j.mser.2011.04.001
56. Kläui M. Head-to-head domain walls in magnetic nanostructures. *J Phys Condens Matter*. (2008) **20**:313001. doi: 10.1088/0953-8984/20/31/313001
57. Thiaville A, Nakatani Y. Domain-wall dynamics in nanowires and nanostrips. In: Hillebrands B, Thiaville A, editors. *Spin Dynamics in Confined Magnetic Structures III. Vol. 101 of Topics in Applied Physics*. Berlin; Heidelberg: Springer (2006). p. 161–205.
58. Kläui M, Vaz CAF, Bland JAC, Heyderman LJ, Nolting F, Pavlovska A, et al. Head-to-head domain-wall phase diagram in mesoscopic ring magnets. *Appl Phys Lett*. (2004) **85**:5637–9. doi: 10.1063/1.1829800
59. Laufenberg M, Backes D, Bührer W, Bedau D, Kläui M, Rüdiger U, et al. Observation of thermally activated domain wall transformations. *Appl Phys Lett*. (2006) **88**:052507. doi: 10.1063/1.2168677
60. Junginger F, Kläui M, Backes D, Krzyk S, Rüdiger U, Kasama T, et al. Quantitative determination of vortex core dimensions in head-to-head domain walls using off-axis electron holography. *Appl Phys Lett*. (2008) **92**:112502. doi: 10.1063/1.2829601
61. Diegel M, Glathe S, Mattheis R, Scherzinger M, Halder E. A new four bit magnetic domain wall based multiturn counter. *IEEE Trans Magneti*. (2009) **45**:3792–5. doi: 10.1109/TMAG.2009.2024426
62. Parkin SSP, Hayashi M, Thomas L. Magnetic domain-wall racetrack memory. *Science* (2008) **320**:190–4. doi: 10.1126/science.1145799
63. Allwood DA, Xiong G, Faulkner CC, Atkinson D, Petit D, Cowburn RP. Magnetic domain-wall logic. *Science* (2005) **309**:1688–92. doi: 10.1126/science.1108813
64. Stein FU, Bocklage L, Weigand M, Meier G. Time-resolved imaging of nonlinear magnetic domain-wall dynamics in ferromagnetic nanowires. *Sci Rep*. (2013) **3**:1737. doi: 10.1038/srep01737
65. Stein FU, Bocklage L, Matsuyama T, Meier G. Generation and annihilation of domain walls in nanowires by localized fields. *Appl Phys Lett*. (2012) **100**:192403. doi: 10.1063/1.4711222
66. Bocklage L, Stein FU, Martens M, Matsuyama T, Meier G. Time structure of fast domain wall creation by localized fields in a magnetic nanowire. *Appl Phys Lett*. (2013) **103**:092406. doi: 10.1063/1.4819729
67. Hankemeier S, Kobs A, Frömter R, Oepen HP. Controlling the properties of vortex domain walls via magnetic seeding fields. *Phys Rev B* (2010) **82**:064414. doi: 10.1103/PhysRevB.82.064414
68. Rhensius J, Heyne L, Backes D, Krzyk S, Heyderman L, Joly L, et al. Imaging of domain wall inertia in permalloy half-ring nanowires by time-resolved photoemission electron microscopy. *Phys Rev Lett*. (2010) **104**:067201. doi: 10.1103/PhysRevLett.104.067201
69. Stein FU, Bocklage L, Weigand M, Meier G. Direct observation of internal vortex domain-wall dynamics. *Phys Rev B* (2014) **89**:024423. doi: 10.1103/PhysRevB.89.024423
70. Kläui M, Vaz CAF, Lopez-Diaz L, Bland JAC. Vortex formation in narrow ferromagnetic rings. *J Phys Condens Matter*. (2003) **15**:R985. doi: 10.1088/0953-8984/15/21/201
71. Rothman J, Kläui M, Lopez-Diaz L, Vaz CAF, Bleloch A, Bland JAC, et al. Observation of a bi-domain state and nucleation free switching in mesoscopic ring magnets. *Phys Rev Lett*. (2001) **86**:1098. doi: 10.1103/PhysRevLett.86.1098
72. Zhu JG, Zheng Y, Prinz GA. Ultrahigh density vertical magnetoresistive random access memory (invited). *J Appl Phys*. (2000) **87**:6668–73. doi: 10.1063/1.372805
73. Negoita M, Hayward TJ, Allwood DA. Controlling domain walls velocities in ferromagnetic ring-shaped nanowires. *Appl Phys Lett*. (2012) **100**:072405. doi: 10.1063/1.3685467
74. Yang T, Pradhan NR, Goldman A, Licht AS, Li Y, Kemei M, et al. Manipulation of magnetization states of ferromagnetic nanorings by an applied azimuthal Oersted field. *Appl Phys Lett*. (2011) **98**:242505. doi: 10.1063/1.3599714
75. Saitoh E, Kawabata M, Harii K, Miyajima H, Yamaoka T. Manipulation of vortex circulation in decentered ferromagnetic nanorings. *J Appl Phys*. (2004) **95**:1986–8. doi: 10.1063/1.1638893
76. Singh DK, Krotkov R, Tuominen MT. Magnetic transitions in ultra-small nanoscopic magnetic rings: Theory and experiments. *Phys Rev B* (2009) **79**:184409. doi: 10.1103/PhysRevB.79.184409
77. Bisig A, Stärk M, Mawass MA, Moutafis C, Rhensius J, Heidler J, et al. Correlation between spin structure oscillations and domain wall velocities. *Nat Commun*. (2013) **4**:3328. doi: 10.1038/ncomms3328
78. Schryer NL, Walker LR. The motion of 180° domain walls in uniform dc magnetic fields. *J Appl Phys*. (1974) **45**:5406–21. doi: 10.1063/1.1663252
79. Albert M, Franchin M, Fischbacher T, Meier G, Fangohr H. Domain wall motion in perpendicular anisotropy nanowires with edge roughness. *J Phys Condens Matter*. (2012) **24**:024219. doi: 10.1088/0953-8984/24/2/024219
80. Mougin A, Cormier M, Adam JP, Metaxas PJ, Ferr J. Domain wall mobility, stability and Walker breakdown in magnetic nanowires. *EPL* (2007) **78**:57007. doi: 10.1209/0295-5075/78/57007
81. Beach GSD, Tsoi M, Erskine JL. Current-induced domain wall motion. *J Magn Magn Mater*. (2008) **320**:1272–81. doi: 10.1016/j.jmmm.2007.12.021
82. Ilgaz D, Kläui M, Heyne L, Boulle O, Zinser F, Krzyk S, et al. Selective domain wall depinning by localized Oersted fields and Joule heating. *Appl Phys Lett*. (2008) **93**:132503. doi: 10.1063/1.2990629
83. Kim JS, Mawass MA, Bisig A, Krüger B, Reeve RM, Schulz T, et al. Synchronous precessional motion of multiple domain walls in a ferromagnetic nanowire by perpendicular field pulses. *Nat Commun*. (2014) **5**:4429. doi: 10.1038/ncomms4429
84. Krüger B, Pfannkuche D, Bolte M, Meier G, Merkt U. Current-driven domain-wall dynamics in curved ferromagnetic nanowires. *Phys Rev B* (2007) **75**:054421. doi: 10.1103/PhysRevB.75.054421
85. You CY, Sung IM, Joe BK. Analytic expression for the temperature of the current-heated nanowire for the current-induced domain wall motion. *Appl Phys Lett*. (2006) **89**:222513. doi: 10.1063/1.2399441
86. You CY, Ha SS. Temperature increment in a current-heated nanowire for current-induced domain wall motion with finite thickness insulator layer. *Appl Phys Lett*. (2007) **91**:022507. doi: 10.1063/1.2754351
87. Junginger F, Kläui M, Backes D, Rüdiger U, Kasama T, Dunin-Borkowski RE, et al. Spin torque and heating effects in current-induced domain wall motion probed by transmission electron microscopy. *Appl Phys Lett*. (2007) **90**:132506. doi: 10.1063/1.2709989
88. Landau L, Lifshitz EM. On the theory of the dispersion of magnetic permeability in ferromagnetic bodies. *Phys Z Sowjetunion* (1935) **8**:153.
89. Gilbert TL. A lagrangian formulation of the gyromagnetic equation of the magnetic field. *Phys Rev*. (1955) **100**:1243.
90. Zhang J, Levy PM, Zhang S, Antropov V. Identification of transverse spin currents in noncollinear magnetic structures. *Phys Rev Lett*. (2004) **93**:256602. doi: 10.1103/PhysRevLett.93.256602

91. Thiaville A, Nakatani Y, Miltat J, Suzuki Y. Micromagnetic understanding of current-driven domain wall motion in patterned nanowires. *EPL* (2005) **69**:990. doi: 10.1209/epl/i2004-10452-6
92. Tatara G, Kohno H, Shibata J. Microscopic approach to current-driven domain wall dynamics. *Phys Rep*. (2008) **468**:213–301. doi: 10.1016/j.physrep.2008.07.003
93. Tatara G, Kohno H. Theory of current-driven domain wall motion: spin transfer versus momentum transfer. *Phys Rev Lett*. (2004) **92**:086601. doi: 10.1103/PhysRevLett.92.086601
94. Tatara G, Takayama T, Kohno H, Shibata J, Nakatani Y, Fukuyama H. Threshold current of domain wall motion under extrinsic pinning, -term and non-adiabaticity. *J Phys Soc Jpn*. (2006) **75**:064708. doi: 10.1143/JPSJ.75.064708
95. Tserkovnyak Y, Brataas A, Bauer GEW. Theory of current-driven magnetization dynamics in inhomogeneous ferromagnets. *J Magn Magn Mater*. (2008) **320**:1282–92. doi: 10.1016/j.jmmm.2007.12.012
96. Vanhaverbeke A, Viret M. Simple model of current-induced spin torque in domain walls. *Phys Rev B* (2007) **75**:024411. doi: 10.1103/PhysRevB.75.024411
97. Waintal X, Viret M. Current-induced distortion of a magnetic domain wall. *EPL* (2004) **65**:427. doi: 10.1209/epl/i2003-10089-y
98. Zhang S, Li Z. Roles of nonequilibrium conduction electrons on the magnetization dynamics of ferromagnets. *Phys Rev Lett*. (2004) **93**:127204. doi: 10.1103/PhysRevLett.93.127204
99. Shibata J, Tatara G, Kohno H. A brief review of field- and current-driven domain-wall motion. *J Phys D Appl Phys*. (2011) **44**:384004. doi: 10.1088/0022-3727/44/38/384004
100. Malinowski G, Boulle O, Kläui M. Current-induced domain wall motion in nanoscale ferromagnetic elements. *J Phys D Appl Phys*. (2011) **44**:384005. doi: 10.1088/0022-3727/44/38/384005
101. Schieback C, Kläui M, Nowak U, Rüdiger U, Nielaba P. Numerical investigation of spin-torque using the Heisenberg model. *Eur Phys J B* (2007) **59**:429–33. doi: 10.1140/epjb/e2007-00062-2
102. Thiaville A, Nakatani Y, Miltat J, Vernier N. Domain wall motion by spin-polarized current: a micromagnetic study. *J Appl Phys*. (2004) **95**:7049–51. doi: 10.1063/1.1667804
103. Barnes SE, Maekawa S. Current-spin coupling for ferromagnetic domain walls in fine wires. *Phys Rev Lett*. (2005) **95**:107204. doi: 10.1103/PhysRevLett.95.107204
104. Kläui M, Laufenberg M, Heyne L, Backes D, Rüdiger U, Vaz CAF, et al. Current-induced vortex nucleation and annihilation in vortex domain walls. *Appl Phys Lett*. (2006) **88**:232507. doi: 10.1063/1.2209177
105. Meier G, Bolte M, Eiselt R, Krüger B, Kim DH, Fischer P. Direct imaging of stochastic domain-wall motion driven by nanosecond current pulses. *Phys Rev Lett*. (2007) **98**:187202. doi: 10.1103/PhysRevLett.98.187202
106. Heyne L, Kläui M, Backes D, Moore TA, Krzyk S, Rüdiger U, et al. Relationship between nonadiabaticity and damping in permalloy studied by current induced spin structure transformations. *Phys Rev Lett*. (2008) **100**:066603. doi: 10.1103/PhysRevLett.100.066603
107. Moore TA, Kläui M, Heyne L, Möhrke P, Backes D, Rhensius J, et al. Scaling of spin relaxation and angular momentum dissipation in permalloy nanowires. *Phys Rev B* (2009) **80**:132403. doi: 10.1103/PhysRevB.80.132403
108. Heyne L, Rhensius J, Bisig A, Krzyk S, Punke P, Kläui M, et al. Direct observation of high velocity current induced domain wall motion. *Appl Phys Lett*. (2010) **96**:032504. doi: 10.1063/1.3291067
109. Bocklage L, Krüger B, Matsuyama T, Bolte M, Merkt U, Pfannkuche D, et al. Dependence of magnetic domain-wall motion on a fast changing current. *Phys Rev Lett*. (2009) **103**:197204. doi: 10.1103/PhysRevLett.103.197204
110. Heyne L, Kläui M, Rhensius J, Le Guyader L, Nolting F. *In situ* contacting and current-injection into samples in photoemission electron microscopes. *Rev Sci Instrum*. (2010) **81**:113707. doi: 10.1063/1.3495967
111. Bailey W, Kabos P, Mancoff F, Russek S. Control of magnetization dynamics in Ni81Fe19 thin films through the use of rare-earth dopants. *IEEE Trans. Magnet*. (2001) **37**:1749–54. doi: 10.1109/20.950957
112. Garate I, Gilmore K, Stiles MD, MacDonald AH. Nonadiabatic spin-transfer torque in real materials. *Phys Rev B* (2009) **79**:104416. doi: 10.1103/PhysRevB.79.104416
113. Krüger B, Najafi M, Bohlens S, Frömter R, Möller DPF, Pfannkuche D. Proposal of a robust measurement scheme for the nonadiabatic spin torque using the displacement of magnetic vortices. *Phys Rev Lett*. (2010) **104**:077201. doi: 10.1103/PhysRevLett.104.077201
114. Heyne L, Rhensius J, Ilgaz D, Bisig A, Rüdiger U, Kläui M, et al. Direct determination of large spin-torque nonadiabaticity in vortex core dynamics. *Phys Rev Lett*. (2010) **105**:187203. doi: 10.1103/PhysRevLett.105.187203
115. Rößler S, Hankemeier S, Krüger B, Balhorn F, Frömter R, Oepen HP. Nonadiabatic spin-transfer torque of magnetic vortex structures in a permalloy square. *Phys Rev B* (2014) **89**:174426. doi: 10.1103/PhysRevB.89.174426
116. Eltschka M, Wötzel M, Rhensius J, Krzyk S, Nowak U, Kläui M, et al. Nonadiabatic spin torque investigated using thermally activated magnetic domain wall dynamics. *Phys Rev Lett*. (2010) **105**:056601. doi: 10.1103/PhysRevLett.105.056601
117. Chapman JN. High resolution imaging of magnetic structures in the transmission electron microscope. *Mater Sci Eng B* (1989) **3**:355–8. doi: 10.1016/0921-5107(89)90140-2
118. Dunin-Borkowski RE, McCartney MR, Smith DJ. *Encyclopedia of Nanoscience and Nanotechnology. Vol. 3*. Stevenson Ranch, CA: American Scientific Publishers (2004).
119. Bolte M, Meier G, Krüger B, Drews A, Eiselt R, Bocklage L, et al. Time-resolved X-ray microscopy of spin-torque-induced magnetic vortex gyration. *Phys Rev Lett*. (2008) **100**:176601. doi: 10.1103/PhysRevLett.100.176601
120. Bisig A, Rhensius J, Kammerer M, Curcic M, Stoll H, Schütz G, et al. Direct imaging of current induced magnetic vortex gyration in an asymmetric potential well. *Appl Phys Lett*. (2010) **96**:152506. doi: 10.1063/1.3373590
121. Krüger B, Drews A, Bolte M, Merkt U, Pfannkuche D, Meier G. Harmonic oscillator model for current- and field-driven magnetic vortices. *Phys Rev B* (2007) **76**:224426. doi: 10.1103/PhysRevB.76.224426
122. Huber DL. Equation of motion of a spin vortex in a two-dimensional planar magnet. *J Appl Phys*. (1982) **53**:1899–1900. doi: 10.1063/1.330661
123. Büttner F, Moutafis C, Schneider M, Krüger B, Günther CM, Geilhufe J, et al. Dynamics and inertia of skyrmionic spin structures. *Nat Phys*. (2015) **11**:225–8. doi: 10.1038/nphys3234
124. Moutafis C, Komineas S, Bland JAC. Dynamics and switching processes for magnetic bubbles in nanoelements. *Phys Rev B* (2009) **79**:224429. doi: 10.1103/PhysRevB.79.224429
125. Makhfudz I, Krüger B, Tchernyshyov O. Inertia and chiral edge modes of a skyrmion magnetic bubble. *Phys Rev Lett*. (2012) **109**:217201. doi: 10.1103/PhysRevLett.109.217201
126. Thiele AA. Applications of the gyrocoupling vector and dissipation dyadic in the dynamics of magnetic domains. *J Appl Phys*. (1974) **45**:377–93. doi: 10.1063/1.1662989
127. Geilhufe J, Pfau B, Schneider M, Büttner F, Günther CM, Werner S, et al. Monolithic focused reference beam X-ray holography. *Nat Commun*. (2014) **5**:4008. doi: 10.1038/ncomms4008
128. Büttner F, Moutafis C, Bisig A, Wohlhüter P, Günther CM, Mohanty J, et al. Magnetic states in low-pinning high-anisotropy material nanostructures suitable for dynamic imaging. *Phys Rev B* (2013) **87**:134422. doi: 10.1103/PhysRevB.87.134422
129. Büttner F. *Topological Mass of Magnetic Skyrmions Probed by Ultrafast Dynamic Imaging*. PhD thesis, Mainz: Johannes Gutenberg University Mainz (2013).

Conflict of Interest Statement: The authors declare that the research was conducted in the absence of any commercial or financial relationships that could be construed as a potential conflict of interest.